

25 **Summary**

26 The remodeling of neurons is a conserved fundamental mechanism underlying nervous system
27 maturation and function. Glial cells are known to clear neuronal debris but also to have an
28 active role in the remodeling process. Developmental axon pruning of *Drosophila* memory
29 center neurons occurs by a degenerative process mediated by infiltrating astrocytes. However,
30 how these glial processes are recruited by the axons is unknown. In an unbiased screen, we
31 identified a new gene (*orion*) which is necessary for both the pruning of some axons and
32 removal of the resulting debris. Orion is secreted from the neurons and bears some features
33 common to the chemokines, a family of chemoattractant cytokines. Thus, chemokine
34 involvement in neuron/glial cell interaction is an evolutionarily ancient mechanism. We
35 propose that Orion is the neuronal signal that elicits astrocyte infiltration required for
36 developmental neuronal remodeling.

37

38

39 **Introduction**

40 Neuronal remodeling is a widely used developmental mechanism, across the animal kingdom,
41 to refine dendrite and axon targeting necessary for the maturation of neural circuits.
42 Importantly, similar molecular and cellular events can occur during neurodevelopmental
43 disorders or after nervous system injury¹⁻⁴. A key role for glial cells in synaptic pruning and
44 critical signaling pathways between glia and neurons have been identified⁴. In *Drosophila*, the
45 mushroom body (MB), a brain memory center, is remodeled at metamorphosis and MB γ
46 neuron pruning occurs by a degenerative mechanism⁵⁻⁸. Astrocytes surrounding the MB have
47 an active role in the process; blocking their infiltration into the MBs prevents remodeling⁹⁻¹².
48 MB γ neuron remodeling relies on two processes: axon fragmentation and the subsequent
49 clearance of axonal debris. Importantly, it has been shown that astrocytes are involved in these
50 two processes and that these two processes can be decoupled¹². Altering the ecdysone signaling
51 in astrocytes, during metamorphosis, results both in a partial axon pruning defect, visualized as
52 either some individual larval axons or as thin bundles of intact larval axons remaining in the
53 adults, and also in a strong defect in clearance of debris, visualized by the presence of clusters
54 of axonal debris. Astrocytes have only a minor role in axon severing as evidenced by the
55 observation that most of the MB γ axons are correctly pruned when ecdysone signaling is
56 altered in these cells. When astrocyte function is blocked, the γ axon-intrinsic fragmentation
57 process remains functional and the majority of axons degenerate.

58 It has been widely proposed that a “find-me/eat-me” signal emanating from the degenerating γ
59 neurons is necessary for astrocyte infiltration^{7,9,13}. However, the nature of this glial recruitment
60 signal is unknown.

61 Here we have identified a new gene (*orion*) by screening for viable ethyl
62 methanesulfonate (EMS)-induced mutations and not for lethal mutations in MB clones as was
63 done previously^{14,15}. This allowed the identification of genes involved in glia cell function by
64 directly screening for defects in MB axon pruning. We found that *orion*^l, a viable X
65 chromosome mutation, is necessary for both the pruning of some γ axons and removal of the
66 resulting debris. We show that Orion is secreted from the neurons, remains near the axon
67 membranes where it associates with infiltrating astrocytes, and is necessary for astrocyte
68 infiltration into the γ bundle. This implies a role for an as-yet-undefined Orion receptor on the
69 surface of the astrocytes. Orion bears some chemokine features, e.g, a CX₃C motif, 3
70 glycosaminoglycan binding consensus sequences that are required for its function. Altogether,
71 our results identify a neuron-secreted extracellular messenger, which is likely to be the long-
72 searched-for signal responsible for astrocyte infiltration and demonstrate its involvement for
73 neuronal remodeling.

74

75 **Results and Discussion**

76 **The *orion* gene is necessary for MB remodeling**

77 Adult *orion*^l individuals showed a clear and highly penetrant MB axon pruning phenotype as
78 revealed by the presence of some adult unpruned vertical γ axons as well as the strong presence
79 of debris (100% of mutant MBs; n = 100) (Fig. 1a, b, Table I and Supplementary Fig.1 and 2).
80 Astrocytes, visualized with *alm-GAL4*, are the major glial subtype responsible for the
81 clearance of the MB axon debris¹². The presence of γ axon debris is a landmark of defective
82 astrocyte function, as was previously described^{11,12}, and is also further shown in this study
83 (Supplementary Fig. 1a-d). The unpruned axon phenotype was particularly apparent during
84 metamorphosis (Fig. 1c-h). At 24 h after puparium formation (APF), although γ axon branches
85 were nearly completely absent in the wild-type control they persisted in the *orion*^l mutant
86 brains, where we also observed a significant accumulation of debris (Fig. 1e, h). The number
87 of unpruned axons at this stage is lower in *orion*^l than in *Hr39*^{C13} where the γ axon-intrinsic
88 process of pruning is blocked (Supplementary Fig. 1 e-g). In addition, the MB dendrite pruning
89 was clearly affected in *orion*^l individuals (Supplementary Fig. 1h-p).

90

91 **The *orion* gene encodes for a CX₃C motif-containing secreted proteins**

92 The *orion*^l EMS mutation was localized by standard duplication and deficiency mapping as
93 well as by whole genome sequencing (Fig. 2a). The *orion* gene (CG2206) encodes two
94 putatively secreted proteins: Orion-A (664 aa) and Orion-B (646 aa), whose mRNAs arise from
95 two different promoters (Fig. 2b-d). We have confirmed that both mRNAs are present in early
96 pupal brains by RT-PCR (data not shown). These two proteins differ in their N-terminal
97 domains and are identical in the remainder of their sequences. The EMS mutation is a G to C
98 nucleotide change inducing the substitution of the glycine (at position 629 for Orion-A and 611
99 for Orion-B) into an aspartic acid. The mutation lies in the common shared part and therefore
100 affects both Orion-A and -B functions. Both isoforms display a signal peptide at their N-termini
101 suggesting that they are secreted. Interestingly, a CX₃C chemokine signature is present in the
102 Orion common region (Fig. 2b, c). Chemokines are a family of chemoattractant cytokines,
103 characterized by a CC, CXC or CX₃C motif, promoting the directional migration of cells within
104 different tissues. Mammalian CX₃CL1 (also known as fractalkine) is involved in, among other
105 contexts, neuron-glia communication¹⁶⁻²⁰. Mammalian Fractalkines display conserved
106 intramolecular disulfide bonds that appear to be conserved with respect to their distance from the
107 CX₃C motif present in both Orion isoforms (Fig. 2c). Fractalkine and its receptor, CX₃CR1,
108 have been recently shown to be required for post-trauma cortical brain neuron microglia-
109 mediated remodeling in a mouse whisker lesioning paradigm²¹. We observed that the change
110 of the CX₃C motif into CX₄C or AX₃C blocked the Orion function necessary for the MB
111 pruning (Supplementary Fig. 3a-c, h-j). Similarly, the removal of the signal peptide also
112 prevented pruning (Supplementary Fig. 3d, h-j). These two results indicate that the Orion
113 isoforms likely act as secreted chemokine-like molecules. We also produced three
114 CRISPR/Cas9-mediated mutations in the *orion* gene, which either delete the common part
115 (*orion*^{ΔC}), the A-specific part (*orion*^{ΔA}) or the B-specific part (*orion*^{ΔB}). Noticeably, *orion*^{ΔC}
116 displayed the same MB pruning phenotype as *orion*^l which is also the same in *orion*^l/*Deficiency*
117 females indicating that *orion*^l and *orion*^{ΔC} are likely null alleles for this phenotype. In contrast,
118 *orion*^{ΔA} and *orion*^{ΔB} have no MB phenotype by themselves indicating the likelihood of
119 functional redundancy between the two proteins in the pruning process (Supplementary Fig. 4).

120

121 **Orion is required and expressed by MB γ axons**

122 Using the GAL4/UAS system²², we found that expression of wild-type *orion* in the *orion*^l MB
123 γ neurons (*201Y-GAL4*) fully rescued the MB mutant phenotype (100% of wild-type MBs n =
124 387; see quantitation in Supplementary Fig. 3h) although wild-type *orion* expression in the
125 astrocytes (*alrm-GAL4*) did not rescue (Fig. 1i-k and Supplementary Fig. 5a-c). *repo-GAL4*

126 could not be used because of lethality when combined with *UAS-orion*. This supports the
127 hypothesis that Orion is produced by axons and, although necessary for astrocyte infiltration,
128 not by astrocytes. Both *UAS-orion-A* and *UAS-orion-B* rescued the *orion^l* pruning phenotype
129 indicating again a likely functional redundancy between the two proteins at least in the pruning
130 process. Complementary to the rescue results, we found that the expression of an *orion*-
131 targeting RNAi in the MBs produced unpruned axons similar to that in *orion^l* although debris
132 are not apparent likely due to an incomplete inactivation of the gene expression by the RNAi
133 (Fig. 11 and Supplementary Fig. 5d). The expression of the same RNAi in the glia had no effect
134 (Supplementary Fig. 5e). Using the mosaic analysis with a repressible cell marker (MARCM
135 ²³), we found that *orion^l* homozygous mutant neuroblast clones of γ neurons, in *orion^{l/+}*
136 phenotypically wild-type individuals, were normally pruned (Supplementary Fig. 6a, b).
137 Therefore, *orion^l* is a non-cell-autonomous mutation which is expected since the Orion proteins
138 are secreted (see below). Orion proteins secreted by the surrounding wild-type axons rescue the
139 pruning defects in the *orion* mutant clones.

140 From our genetic data, *orion* expression is expected in the γ neurons. The fine temporal
141 transcriptional landscape of MB γ neurons was recently described and a corresponding resource
142 is freely accessible²⁴. Noteworthy, *orion* is transcribed at 0h APF and dramatically decreases at
143 9h APF with a peak at 3h APF (Supplementary Fig. 7). The nuclear receptors *EcR-B1* and its
144 target *Sox14* are key transcriptional factors required for MB neuronal remodeling^{6,7}. *orion* was
145 found to be a likely transcriptional target of EcR-B1 and Sox14 ²⁴ and this is also consistent
146 with earlier microarray analysis observations²⁵. Noticeably, forced expression of *UAS-EcR-B1*
147 in the MBs did not rescue the *orion* mutant phenotype and EcR-B1 expression, in the MB
148 nuclei, is not altered in *orion^l* individuals (Supplementary Fig. 6c, f). Furthermore, the
149 unpruned axon phenotype produced by *orion* RNAi is rescued by forced expression of *EcR-B1*
150 in the MBs (Supplementary Fig. 3h). Therefore, our genetic interaction analyses support *orion*
151 being downstream of *EcR-B1*.

152

153 **Orion is secreted by MB γ axons**

154 We focused our further molecular and cellular work on Orion-B alone since a functional
155 redundancy between the two isoforms was apparent. We expressed the Orion-B protein in the
156 γ neurons using an *UAS-orion-B-Myc* insert and the *201Y-GAL4* driver. Orion-B was seen along
157 the MB lobes and at short distances away from the axons as visualized by anti-Myc staining
158 (Fig. 3). In addition, anti-Myc staining was particularly clear at the tip of the lobes indicating
159 the secretion of Orion-B (Fig. 3a, d, g, j, k). Synaptic terminals are condensed in the γ axon

160 varicosities that disappear progressively during remodeling and hole-like structures
161 corresponding to the vestiges of disappeared varicosities can be observed at 6 h APF⁹. We noted
162 the presence of secreted Myc-labelled Orion-B inside these hole-like structures (Fig. 3b, e, h).
163 The secretion of the Orion proteins should be under the control of their signal peptide and
164 therefore, Orion proteins lacking their signal peptide (Δ SP) should not show this “secretion”
165 phenotype. When *UAS-orion-B-Myc- Δ SP* was expressed, Orion-B was not observed outside of
166 the axons or in the hole-like structures (Fig. 3c, f, i). We also excluded the possibility that this
167 “secretion” phenotype was due to some peculiarities of the Myc labelling by using a *UAS-drl-*
168 *Myc* construct²⁶. Drl is a membrane-bound receptor tyrosine kinase and Drl-Myc staining,
169 unlike Orion-B, was not observed outside of the axons or in the hole-like structures
170 (Supplementary Fig. 6g-l). Finally, the presence of Myc-labelled Orion-B secreted protein not
171 associated with GFP-labelled axon membranes can be observed outside of the γ axon bundle in
172 3D reconstructing images (Fig. 3j, k).

173

174 **Orion is required for the infiltration of astrocytes into the MB γ bundle**

175 Since glial cells are likely directly involved in the *orion*¹ pruning phenotype, we examined their
176 behavior early during the pruning process. At 6 h APF the axon pruning process starts and is
177 complete by 24 h APF but the presence of glial cells in the vicinity of the wild-type γ lobes is
178 already clearly apparent at 6 h APF⁹. We examined glial cells visualized by a membrane-
179 targeted GFP (*UAS-mGFP*) under the control of *repo-GAL4* and co-stained the γ axons with
180 anti-Fas2. At 6 h APF a striking difference was noted between wild-type and *orion*¹ brains.
181 Unlike in the wild-type control, there is essentially no glial cell invasion of the γ bundle in the
182 mutant (Fig. 4a-c). Interestingly, glial infiltration was not observed in *orion*¹ neither at 12 h
183 APF nor at 24 h APF (Supplementary Fig. 8 a-h) suggesting that glial cells never infiltrate MBs
184 in mutant individuals. We also ruled out the possibility that this lack of glial cell infiltration
185 was due to a lower number of astrocytes in mutant versus wild-type brains (Supplementary Fig.
186 8i, j).

187 We also examined the proximity between MB-secreted Orion-Myc and astrocytes, as
188 inferred from the shape of the glial cells, labelled with the anti-Drpr antibody at 6 h APF (Fig.
189 4d-f). We looked at the distribution along the vertical γ lobes (60 μ m of distance, see Methods)
190 of Orion-B-Myc (secreted) and of Orion-B- Δ SP-Myc (not secreted), in an otherwise wild-type
191 background. We quantified only from images where an astrocyte sat on the top of the vertical
192 lobe. A peak of Orion-Myc localization was always found (n = 10) in the region close to the
193 astrocyte (less than 7 μ m) when secreted Orion-B-Myc was quantified (Fig. 4g, i). However,

194 this was not the case ($n = 9$) when Orion-B- Δ SP-Myc was quantified (Fig. 4h, j). This strongly
195 suggests that astrocytic processes may be “attracted” by secreted Orion.

196 Moreover, we observed that secreted Orion stays close to axon membranes
197 (Supplementary Fig. 9a-f). Protein, in particular chemokine, localization to membranes is often
198 mediated by glycosaminoglycans (GAGs), a family of highly anionic polysaccharides that
199 occur both at the cell surface and within the extracellular matrix. GAGs, to which all
200 chemokines bind, ensure that these signaling proteins are presented at the correct site and time
201 in order to mediate their functions²⁷. We identified three consensus sequences for GAG linkage
202 in the common part of Orion (Fig. 2d). We mutated these sequences individually and assayed
203 the mutant proteins for their ability to rescue the *orion*¹ pruning deficit *in vivo*. The three GAG
204 sites are required for full Orion function, although mutating only GAG3 produced a strong
205 mutant phenotype (Supplementary Fig. 3e-j).

206 Our findings imply a role for an as-yet-undefined Orion receptor on the surface of the
207 glial cells. The glial receptor *draper* (*drpr*) seemed an obvious candidate^{13,28-30}, although Drpr
208 ligands unrelated to Orion have been identified^{31,32}. The MB remodeling phenotypes in *orion*¹
209 and *drpr* ^{Δ 5} are, however, different; only *orion*¹ displayed unpruned axons and the *drpr* mutant
210 phenotype does not persist throughout adulthood¹³ (Table I and Supplementary Fig. 1).
211 Strikingly, using *UAS-mGFP* driven by *201Y-GAL4*, instead of *Fas2*, where the labelling of $\alpha\beta$
212 axons often masks individual unpruned γ axons, allowed us to observe occasionally unpruned
213 axons in *drpr* ^{Δ 5} one-week-old post-eclosion brains (Table I and Supplementary Fig. 2)
214 indicating a certain degree of undescribed axon persistence in the mutant background. In
215 addition, our data indicate that Orion does not induce the Drpr signaling pathway
216 (Supplementary Fig. 10). This suggests that Drpr is not an, or at least not the sole, Orion
217 receptor.

218 We have uncovered a neuronally-secreted chemokine-like protein acting as a “find-
219 me/eat-me” signal involved in the neuron-glia crosstalk required for axon pruning during
220 developmental neuron remodeling. To the best of our knowledge, chemokine-like signaling in
221 insects was not described previously and furthermore our results point to an unexpected
222 conservation of chemokine CX₃C signaling in modulation of neural circuits.

223

224 **Methods**

225 **Drosophila stocks**

226 All crosses were performed using standard culture medium at 25 °C. Except where otherwise
227 stated, alleles have been described previously (<http://flystocks.bio.indiana.edu>). The following

228 alleles were used. *orion^l*, *orion^{ΔA}*, *orion^{ΔB}* and *orion^{ΔC}* were generated in this study. *drpr^{Δ5rec8}*
229 was found to have an unlinked lethal mutation which was removed by standard mitotic
230 recombination over a wild-type chromosome^{28,29}. Animals bearing this version of *drpr^{Δ5}*
231 survive to adult stages and were used for this work. The following transgenes were used. *UAS-*
232 *orion-RNAi* (VDRC stock 30843) and 2x *UAS-drl-myc²⁶*, *10X-Stat92E-GFP³³*. *UAS-orion-A*,
233 *UAS-orion-A-myc*, *UAS-orion-B*, *UAS-orion-B-myc*, *UAS-orion-B-Mut AX3C-myc*, *UAS-*
234 *orion-B-Mut CX4C-myc*, *UAS-orion-B-ΔSP-myc*, *UAS-orion-B-Mut GAG1-myc*, *UAS-orion-B-*
235 *Mut GAG2-myc* and *UAS-orion-B-Mut GAG3-myc* were generated in this study. We used three
236 GAL4 lines: *201Y-GAL4* expressed in γ MB neurons, *alrm-GAL4* expressed exclusively in glial
237 astrocytes³⁴ and the pan-glial driver *repo-GAL4* expressed in all glia³⁵.

238

239 **Mutagenesis and screening**

240 EMS mutagenesis was carried out following the published procedure³⁶. EMS treated *y w^{67c23}*
241 *sn³ FRT19A* males were crossed to *FM7c/ph⁰ w* females and stocks, coming from single *y w^{67c23}*
242 *sn³ FRT19A/ FM7c* female crossed to *FM7c* males, were generated. Only viable *y w^{67c23} sn³*
243 *FRT19A* chromosome bearing stocks were kept and *y w^{67c23} sn³ FRT19A; UAS-mCD8-GFP*
244 *201Y-GAL4* /+ adult males from each stock were screened for MB neuronal remodeling defect
245 with an epi-fluorescence microscope (Leica DM 6000).

246

247 **Mapping of *orion***

248 To broadly map the location of the EMS-induced mutation on the X chromosome we used
249 males from the stocks described in the X-chromosome duplication kit (Bloomington Stock
250 Center) that we crossed with *orion^l; UAS-mCD8-GFP 201Y-GAL4* females. Dp(1; Y)BSC346
251 (stock 36487) completely rescued the *orion^l* γ axon unpruned phenotype. This duplication is
252 located at 6D3-6E2; 7D18 on the X chromosome. We then used smaller duplications covering
253 this region. Thus, duplications Dp(1 ;3)DC496 (stock 33489) and Dp(1;3)DC183 (stock 32271)
254 also rescued the *orion^l* mutant phenotype. However duplication Dp(1;3)DC184 (stock 30312)
255 did not rescue the mutant phenotype. Overlapping of duplications indicates that the EMS
256 mutation was located between 7C9 and 7D2 which comprises 72 kb. In addition, deficiency
257 Def(1)C128 (stock 949, Bloomington Stock Center) which expand from 7D1 to 7D5-D6
258 complements *orion^l* contrarily to deficiency Def(1)BSC622 (stock 25697, Bloomington Stock
259 Center) which does not (see Fig. 2a). We named this gene *orion* since the debris present in
260 mutant MBs resembles a star constellation.

261

262 **Whole-Genome Sequencing**

263 Gene mutation responsible for the unpruned γ axon phenotype was precisely located through
264 the application of next generation sequencing. Genomic DNA was extracted from 30 adult
265 females (mutant and control) and directly sequenced on a HiSeq2000 next-generation
266 sequencing platform (Illumina). Bioinformatics analysis for read alignment and variant
267 investigation was carried out through the 72 kb selected by duplication mapping (see above) at
268 the University of Miami Miller School of Medicine, Center for Genome Technology.

269

270 **Signal peptide and transmembrane protein domain research**

271 For prediction of signal peptide sequences, we used the PrediSi website³⁷:
272 <http://www.predisi.de>; for transmembrane domains, we used the TMHMM Server, v 2.0³⁸:
273 <http://www.cbs.dtu.dk/services/TMHMM/>

274

275 **Orion and fractalkine alignments**

276 The sequence of the region common to both Orion isoforms containing the CX₃C motifs and
277 the likely conserved CX₃C-downstream cysteines and those of the human, mouse and chicken
278 fractalkine were aligned using the AlignX plug-in in the VectorNTi software package
279 (InVitrogen) without permitting introduction of spaces or deletions.

280

281 **GAG binding site research**

282 Identification of GAG binding sites in proteins, in absence of structural data, is complicated by
283 the diversity of both GAG structure and GAG binding proteins. Previous work based on
284 heparin-binding protein sequence comparisons led to the proposition of two GAG binding
285 consensus sequences, the XBBXBX and XBBBXXBX motifs (where B and X stand for basic
286 and neutral/hydrophobic amino acids respectively). A number of closely related basic clusters,
287 including XBBXBXB were next experimentally identified³⁹. Visual examination of the
288 Orion-B sequences returned three such clusters (XBBXXBXXBXXBX: residues 242-254;
289 XBBXBX: residues 416-421 and XBBXBXBX: residues 547-554, numbering includes the
290 peptide signal see Fig. 2d), which are also present in Orion-A.

291

292 **CRISPR-Cas9 strategy**

293 All guide RNA sequences (sgRNA) were selected using the algorithm
294 targetfinder.flycrispr.neuro.brown.edu/ containing 20 nucleotides each (PAM excluded) and
295 are predicted to have zero off-targets. We selected three pairs of sgRNA. Each pair is targeting

296 either the A specific region of *orion*, the B specific region of *orion* or the C common region of
297 the two isoforms. We used the following oligonucleotide sequences:

298 CRISPR-1 orion A fwd :

299 TATATAGGAAAGATATCCGGGTGAACTTCATTTGCGTTTTGATTTTCAGGTTTTAG

300 AGCTAGAAATAGCAAG

301 CRISPR-1 orion A rev :

302 ATTTTAACTTGCTATTTCTAGCTCTAAAACGCTGTTGGAGTAGATTGGTGGACGTT

303 AAATTGAAAATAGGTC

304 CRISPR-1 orion B fwd :

305 TATATAGGAAAGATATCCGGGTGAACTTCGTGAAATCTCAGCTGTATCGGTTTTA

306 GAGCTAGAAATAGCAAG

307 CRISPR-1 orion B rev :

308 ATTTTAACTTGCTATTTCTAGCTCTAAAACGCTAGATTTAAAACGGCAAGGACGTT

309 AAATTGAAAATAGGTC

310 CRISPR-1 orion commun region C fwd :

311 TATATAGGAAAGATATCCGGGTGAACTTCACCTGGTAAAGAATGCCAGAGTTTTA

312 GAGCTAGAAATAGCAAG

313 CRISPR-1 orion commun region C rev :

314 ATTTTAACTTGCTATTTCTAGCTCTAAAACCTTCGCGTCCAGGTGAGTCTGACGTT

315 AAATTGAAAATAGGTC

316 We introduced two sgRNA sequences into pCFD4⁴⁰, a gift from Simon Bullock (Addgene
317 plasmid # 49411) by Gibson Assembly (New England Biolabs) following the detailed protocol
318 at crisprflydesign.org. For PCR amplification, we used the protocol described on that website.
319 Construct injection was performed by Bestgene (Chino Hills, CA) and all the transgenes were
320 inserted into the same attP site (VK00027 at 89E11). Transgenic males expressing the different
321 *orion* sgRNAs were crossed to *y nos-Cas9 w** females bearing an isogenized X chromosome.
322 100 crosses were set up for each sgRNA pair, with up to 5 males containing both the sgRNAs
323 and *nos-Cas9*, and 5 *FM7c/ph⁰ w* females. From each cross, a single *y nos-Cas9 w* /FM7c*
324 female was crossed with *FM7c* males to make a stock which was validated for the presence of
325 an indel by genomic PCR with primers flanking the anticipated deletion and the precise
326 endpoints of the deletion were determined by sequencing (Genewiz, France) using *orion*
327 specific primers.

328

329 **Adult brain dissection, immunostaining and MARCM mosaic analysis**

330 Adult fly heads and thoraxes were fixed for 1 h in 3.7% formaldehyde in PBS and brains were
331 dissected in PBS. For larval and pupal brains, brains were first dissected in PBS and then fixed
332 for 15 min in 3.7% formaldehyde in PBS. They were then treated for immunostaining as
333 previously described^{23,41}. Antibodies, obtained from the Developmental Studies Hybridoma
334 Bank, were used at the following dilutions: Mouse monoclonal anti-Fas2 (1D4) 1:10, mouse
335 monoclonal anti-Draper (8A1), 1:400 and mouse monoclonal anti-Repo (8D1.2) 1:10. Mouse
336 monoclonal primary antibody against EcR-B1 (AD4.4) was used at 1:5.000⁴². Polyclonal
337 mouse (Abcam, (9E10) ab32) and Rabbit (Cell Signaling 7D10) anti-Myc antibodies were used
338 at 1: 1000 and 1: 500, respectively. Goat secondary antibodies conjugated to Cy3, Alexa 488
339 and Cy5 against mouse or rabbit IgG (Jackson ImmunoResearch laboratory) were used at 1:300
340 for detection. To generate clones in the MB, we used the Mosaic Analysis with a Reversible
341 Cell Marker (MARCM) technique²³. First instar larvae were heat-shocked at 37°C for 1 h. Adult
342 brains were fixed for 15 min in 3,7% formaldehyde in PBS before dissection and GFP
343 visualization.

344

345 **Microscopy and image processing**

346 Images were acquired at room temperature using a Zeiss LSM 780 laser scanning confocal
347 microscope (MRI Platform, Institute of Human Genetics, Montpellier, France) equipped with a
348 40x PLAN apochromatic 1.3 oil-immersion differential interference contrast objective lens.
349 The immersion oil used was Immersol 518F. The acquisition software used was Zen 2011
350 (black edition). Contrast and relative intensities of the green (GFP), of the red (Cy3) and of the
351 blue (Cy5 and Alexa 488) channels were processed with ImageJ and Fiji software. Settings
352 were optimized for detection without saturating the signal. For each set of figures settings were
353 constants. However, since the expression of the Orion-B-Myc- Δ SP protein is lower than the
354 one of the Orion-B-Myc (as shown in the western blot and its quantitation Supplementary Fig.
355 3 i-j), the levels of red were increased in this particular case in order to get similar levels than
356 in Orion-B-Myc. We used the Imaris (Bitplane) software to generate a pseudo-3D structure of
357 Orion-secreting γ axons (Imaris surface tool). We created two 3D surfaces, from regular
358 confocal images, defining the axonal domain (green) and the Orion secretion domain (red).

359

360 **Quantitation of immunolabelling**

361 To quantify unpruned γ axons we established three categories of phenotypes: “none”, when no
362 unpruned axons are observed, “weak”, when few unpruned individual axons or thin axon

363 bundles are observed in the dorsal lobe and “strong”, when >50% of the axons are unpruned.
364 In this last category, the percentage of unpruned axons is estimated by the width of the
365 corresponding medial bundle compared with the width of the medial pruned axon bundle⁴¹. For
366 debris quantification we established five categories : none, scattered dots, mild, intermediary
367 and strong based on the location and size of the debris clusters¹¹. In \geq one-week-old adults,
368 “none” means absence of debris. In \leq two-hours-old adults “scattered dots” means some
369 individual debris can be observed. We considered “mild”, if debris clusters (clusters $> 5 \mu\text{m}^2$)
370 appear only at one location, “intermediary”, at two locations and “strong” at three locations of
371 the MB. Three debris locations were considered: the tip of the vertical lobe, the tip of the medial
372 lobe and around the heel (bifurcation site of γ axons into dorsal and medial).
373 For EcR-B1 signal quantitation, we performed 5 measurements for each picture (Intensity 1,...,
374 5) in the nuclei of GFP positive cell bodies and the same number of measurements in
375 background using confocal single slices. The mean of these background measurements is called
376 mean background. We then subtracted intensities of mean background from each intensity value
377 (Intensity 1,...,5 minus mean background) to obtain normalized intensity values. Finally, we
378 compared normalized intensity values between two genetic conditions. We proceeded similarly
379 for Draper and STAT-GFP signal quantitation, but staining was quantified in the astrocyte
380 cytoplasm located in the immediate vicinity of the γ dorsal lobe. Quantitation of intensity was
381 performed using ImageJ software.

382 To quantify the Myc signal in the γ vertical lobe, we traced a 60 μm line on the Cy3 red
383 Z-stack and used the Plot Profile function of ImageJ to create a plot of intensity values across
384 the line. The top of the line (0 μm) was located at the tip of the γ vertical lobe and the bottom
385 of the line (60 μm) at the branching point of the two γ lobes. Only images containing an
386 astrocyte sitting at the top of the γ vertical lobe were used to quantify Myc expression levels in
387 *orion-B* and *orion-B- Δ SP* expressing MBs.

388 To quantify the number of astrocytes around the γ lobes, we counted the number of glial
389 nuclei, as labelled with anti-Repo antibody, contained in GFP-positive astrocyte cytoplasm
390 labelled with *UAS-mCD8-GFP* driven by *alrm-GAL4*. We only counted nuclei contained within
391 a circle of 70 μm of diameter centered in the middle of the vertical γ lobe tips.

392

393 **UAS constructs**

394 The *orion-A cDNA* inserted in the pOT2 plasmid (clone LD24308) was obtained from Berkeley
395 Drosophila Genome Project (BDGP). Initial *Orion-B cDNA* as well as the *Orion-B cDNAs*

396 containing mutations at the CX₃C and the GAG sites or lacking the signal peptide were
397 produced at GenScript (Piscataway, NJ) in the pcDNA3.1-C-(k)DYK vector. The *Orion-B*
398 *cDNAs* contained the following mutations:

399 To remove the signal peptide, we removed sequence: GCGCCGCCTTTCGGATTATTAGCTGCT
400 GTTGTGCTGTTCTTGTACGCTTGTGATTTGTGGAAATA located after the first ATG.

401 At the CX₃C site: In AX₃C we exchanged TGC to GCC. In CX₄C, we added an additional Ala
402 (GCC) to get CAX₃C.

403 To mutate the putative GAG binding sites we exchanged Lys and Arg by Ala at the
404 corresponding sites: **AAGAGGACGGAACGCACACTAAAATACTCAAG**;

405 **AAGCGCAACCGA** and **CGCAGGGAGAACTGCGT** to

406 **GCCGCCACGGAAGCCACACTAGCCATACTCAAG**,

407 **GCCGCCAACGCC** and **GCCGCCGAGGCCCTGGCC** respectively for mutations in GAG1,

408 GAG2 and GAG3.

409 The different constructs were amplified by PCR using forward primers containing
410 sequences CACCaaaacATG (where ATG encodes the first Methionine) followed by the
411 specific *orion-A* or *orion-B cDNA* sequences and including or not nucleotides corresponding to
412 the STOP codon at the reverse primers resulting in transgenes without and with a MYC-tag
413 respectively.

414 To amplify orion-A we used as forward primers (F):

415 F: CACCAAAACATGGAGATTTATAAATTGGGTACTTCCCCT

416 To amplify orion-B we used:

417 F: CACCAAAACATGGCGCCGCCTTTCGGATTATTA

418 For both we used the same reverse oligonucleotide (R):

419 R containing stop: TTAGAATCTATTCTTTGGCACCTGAACGT

420 R without stop: GAATCTATTCTTTGGCACCTGAACGT

421 Amplified cDNA was processed for pENTR/D-TOPO cloning (ThermoFisher
422 Scientific, K240020) and constructs were subsequently sequenced (Genewiz, France). We used
423 the Gateway LR clonase enzyme mix (ThermoFisher Scientific, 11791019) to recombine the
424 inserts into the destination UAS vector pJFRC81-GW-2xMyc (L. G. F., unpublished) which
425 was generated from pJFRC81-10XUAS-IVS-Syn21-GFP-p10 (Addgene plasmid 36462
426 deposited by G. Rubin⁴³) by replacing the GFP ORF with a Gateway cassette adding on a C-
427 terminal 2x Myc tag. *orion-A*, *orion-B* and Myc-tagged constructs (*orion A*, *orion B*, and *orion-*
428 *B mutants*) transgenic fly lines (UASs) were generated at BestGene and all the transgenes were
429 inserted into the same attP site (VK00027 in 89E11). All the crosses involving the UAS-GAL4

430 system were performed at 25°C except for *UAS-orion-A* and *201Y-GAL4* which were performed
431 at 18°C.

432

433 **Western analysis**

434 Five larval heads were homogenized in an Eppendorf tube containing 20 µl of 3X sample buffer
435 (2% SDS, 0.125 M Tris-HCl pH 6.9, 5% β-mercaptoethanol, 20% glycerol, bromophenol blue)
436 and proteins were separated by SDS-PAGE. After electrotransfer to nitrocellulose, the blot was
437 blocked in PBS, 0.5% Tween-20, 5% milk. The Orion-Myc and Tubulin proteins were detected
438 using a mouse anti-Myc antibody (clone 9E10, AbCam) and an anti-Tubulin antibody (Sigma,
439 T5168) at 1/1000 and 1/10.000 respectively in PBS, 0.5% Tween-20, 5% milk and revealed
440 using anti-mouse Ig horseradish peroxidase (1:10.000) and an ECL kit (Amersham). Band
441 intensities were normalized to the corresponding tubulin band intensity using the ImageJ
442 software.

443

444 **Statistics**

445 Comparison between two groups expressing a qualitative variable was analyzed for statistical
446 significance using the Fisher's exact test for a 2x3 contingency table
447 (<https://www.danielsoper.com/statcalc/calculator.aspx?id=58>). Comparison of two groups
448 expressing a quantitative variable was analyzed using the two-tailed non-parametric Mann-
449 Whitney *U* test (<https://www.socscistatistics.com/tests/mannwhitney/Default2.aspx>). Values of
450 $p < 0.05$ were considered to be significant. Graphs were performed using the GraphPad Prism
451 software (version 8.1.1).

452

453 **References**

- 454 1 Luo, L. & O'Leary, D. D. Axon retraction and degeneration in development and disease.
455 *Annu Rev Neurosci* **28**, 127-156 (2005).
- 456 2 Neukomm, L. J. & Freeman, M. R. Diverse cellular and molecular modes of axon
457 degeneration. *Trends Cell Biol* **24**, 515-523, doi:10.1016/j.tcb.2014.04.003 (2014).
- 458 3 Schuldiner, O. & Yaron, A. Mechanisms of developmental neurite pruning. *Cell Mol Life*
459 *Sci* **72**, 101-119, doi:10.1007/s00018-014-1729-6 (2015).
- 460 4 Neniskyte, U. & Gross, C. T. Errant gardeners: glial-cell-dependent synaptic pruning
461 and neurodevelopmental disorders. *Nat Rev Neurosci* **18**, 658-670,
462 doi:10.1038/nrn.2017.110 (2017).
- 463 5 Watts, R. J., Hoopfer, E. D. & Luo, L. Axon pruning during *Drosophila* metamorphosis:
464 evidence for local degeneration and requirement of the ubiquitin-proteasome system.
465 *Neuron* **38**, 871-885 (2003).

- 466 6 Yu, F. & Schuldiner, O. Axon and dendrite pruning in *Drosophila*. *Curr Opin Neurobiol*
467 **27**, 192-198, doi:10.1016/j.conb.2014.04.005 (2014).
- 468 7 Boulanger, A. & Dura, J. M. Nuclear receptors and *Drosophila* neuronal remodeling.
469 *Biochim Biophys Acta* **1849**, 187-195, doi:10.1016/j.bbagr.2014.05.024 (2015).
- 470 8 Yaniv, S. P. & Schuldiner, O. A fly's view of neuronal remodeling. *Wiley Interdiscip Rev*
471 *Dev Biol* **5**, 618-635, doi:10.1002/wdev.241 (2016).
- 472 9 Awasaki, T. & Ito, K. Engulfing action of glial cells is required for programmed axon
473 pruning during *Drosophila* metamorphosis. *Curr Biol* **14**, 668-677,
474 doi:10.1016/j.cub.2004.04.001
475 S0960982204002544 [pii] (2004).
- 476 10 Watts, R. J., Schuldiner, O., Perrino, J., Larsen, C. & Luo, L. Glia engulf degenerating
477 axons during developmental axon pruning. *Curr Biol* **14**, 678-684 (2004).
- 478 11 Tasdemir-Yilmaz, O. E. & Freeman, M. R. Astrocytes engage unique molecular
479 programs to engulf pruned neuronal debris from distinct subsets of neurons. *Genes*
480 *Dev* **28**, 20-33, doi:10.1101/gad.229518.113 (2014).
- 481 12 Hakim, Y., Yaniv, S. P. & Schuldiner, O. Astrocytes play a key role in *Drosophila*
482 mushroom body axon pruning. *PLoS One* **9**, e86178,
483 doi:10.1371/journal.pone.0086178 (2014).
- 484 13 Awasaki, T. *et al.* Essential role of the apoptotic cell engulfment genes *draper* and *ced-*
485 *6* in programmed axon pruning during *Drosophila* metamorphosis. *Neuron* **50**, 855-867
486 (2006).
- 487 14 Lee, T., Marticke, S., Sung, C., Robinow, S. & Luo, L. Cell-autonomous requirement of
488 the USP/EcR-B ecdysone receptor for mushroom body neuronal remodeling in
489 *Drosophila*. *Neuron* **28**, 807-818 (2000).
- 490 15 Zheng, X. *et al.* TGF-beta signaling activates steroid hormone receptor expression
491 during neuronal remodeling in the *Drosophila* brain. *Cell* **112**, 303-315 (2003).
- 492 16 Paolicelli, R. C., Bisht, K. & Tremblay, M. E. Fractalkine regulation of microglial
493 physiology and consequences on the brain and behavior. *Front Cell Neurosci* **8**, 129,
494 doi:10.3389/fncel.2014.00129 (2014).
- 495 17 Arnoux, I. & Audinat, E. Fractalkine Signaling and Microglia Functions in the Developing
496 Brain. *Neural Plast* **2015**, 689404, doi:10.1155/2015/689404 (2015).
- 497 18 Werneburg, S., Feinberg, P. A., Johnson, K. M. & Schafer, D. P. A microglia-cytokine axis
498 to modulate synaptic connectivity and function. *Curr Opin Neurobiol* **47**, 138-145,
499 doi:10.1016/j.conb.2017.10.002 (2017).
- 500 19 Luo, P., Chu, S. F., Zhang, Z., Xia, C. Y. & Chen, N. H. Fractalkine/CX3CR1 is involved in
501 the cross-talk between neuron and glia in neurological diseases. *Brain Res Bull* **146**, 12-
502 21, doi:10.1016/j.brainresbull.2018.11.017 (2019).
- 503 20 Wilton, D. K., Dissing-Olesen, L. & Stevens, B. Neuron-Glia Signaling in Synapse
504 Elimination. *Annu Rev Neurosci* **42**, 107-127, doi:10.1146/annurev-neuro-070918-
505 050306 (2019).
- 506 21 Gunner, G. *et al.* Sensory lesioning induces microglial synapse elimination via ADAM10
507 and fractalkine signaling. *Nat Neurosci* **22**, 1075-1088, doi:10.1038/s41593-019-0419-
508 y (2019).
- 509 22 Brand, A. H. & Perrimon, N. Targeted gene expression as a means of altering cell fates
510 and generating dominant phenotypes. *Development* **118**, 401-415 (1993).
- 511 23 Lee, T. & Luo, L. Mosaic analysis with a repressible cell marker for studies of gene
512 function in neuronal morphogenesis. *Neuron* **22**, 451-461 (1999).

- 513 24 Alyagor, I. *et al.* Combining Developmental and Perturbation-Seq Uncovers
514 Transcriptional Modules Orchestrating Neuronal Remodeling. *Dev Cell* **47**, 38-52 e36,
515 doi:10.1016/j.devcel.2018.09.013 (2018).
- 516 25 Hoopfer, E. D., Penton, A., Watts, R. J. & Luo, L. Genomic analysis of Drosophila
517 neuronal remodeling: a role for the RNA-binding protein Boule as a negative regulator
518 of axon pruning. *J Neurosci* **28**, 6092-6103 (2008).
- 519 26 Reynaud, E. *et al.* Guidance of Drosophila Mushroom Body Axons Depends upon DRL-
520 Wnt Receptor Cleavage in the Brain Dorsomedial Lineage Precursors. *Cell Rep* **11**,
521 1293-1304, doi:10.1016/j.celrep.2015.04.035 (2015).
- 522 27 Monneau, Y., Arenzana-Seisdedos, F. & Lortat-Jacob, H. The sweet spot: how GAGs
523 help chemokines guide migrating cells. *J Leukoc Biol* **99**, 935-953,
524 doi:10.1189/jlb.3MR0915-440R (2016).
- 525 28 Freeman, M. R., Delrow, J., Kim, J., Johnson, E. & Doe, C. Q. Unwrapping glial biology:
526 Gcm target genes regulating glial development, diversification, and function. *Neuron*
527 **38**, 567-580, doi:10.1016/s0896-6273(03)00289-7 (2003).
- 528 29 MacDonald, J. M. *et al.* The Drosophila cell corpse engulfment receptor Draper
529 mediates glial clearance of severed axons. *Neuron* **50**, 869-881,
530 doi:10.1016/j.neuron.2006.04.028 (2006).
- 531 30 Musashe, D. T., Purice, M. D., Speese, S. D., Doherty, J. & Logan, M. A. Insulin-like
532 Signaling Promotes Glial Phagocytic Clearance of Degenerating Axons through
533 Regulation of Draper. *Cell Rep* **16**, 1838-1850, doi:10.1016/j.celrep.2016.07.022
534 (2016).
- 535 31 Kuraishi, T. *et al.* Pretaporter, a Drosophila protein serving as a ligand for Draper in the
536 phagocytosis of apoptotic cells. *EMBO J* **28**, 3868-3878, doi:10.1038/emboj.2009.343
537 (2009).
- 538 32 Lin, L. *et al.* Complement-Related Regulates Autophagy in Neighboring Cells. *Cell* **170**,
539 158-171 e158, doi:10.1016/j.cell.2017.06.018 (2017).
- 540 33 Bach, E. A. *et al.* GFP reporters detect the activation of the Drosophila JAK/STAT
541 pathway in vivo. *Gene Expr Patterns* **7**, 323-331, doi:10.1016/j.modgep.2006.08.003
542 (2007).
- 543 34 Doherty, J., Logan, M. A., Tasdemir, O. E. & Freeman, M. R. Ensheathing glia function
544 as phagocytes in the adult Drosophila brain. *J Neurosci* **29**, 4768-4781, doi:29/15/4768
545 [pii]
546 10.1523/JNEUROSCI.5951-08.2009 (2009).
- 547 35 Sepp, K. J., Schulte, J. & Auld, V. J. Developmental dynamics of peripheral glia in
548 Drosophila melanogaster. *Glia* **30**, 122-133 (2000).
- 549 36 Lewis, E. B. & Bacher, F. Method of feeding ethyl methane sulfonate (EMS) to
550 Drosophila males. *Dros. Inf. Serv.*, 193 (1968).
- 551 37 Hiller, K., Grote, A., Scheer, M., Munch, R. & Jahn, D. PrediSi: prediction of signal
552 peptides and their cleavage positions. *Nucleic Acids Res* **32**, W375-379,
553 doi:10.1093/nar/gkh378 (2004).
- 554 38 Krogh, A., Larsson, B., von Heijne, G. & Sonnhammer, E. L. Predicting transmembrane
555 protein topology with a hidden Markov model: application to complete genomes. *J*
556 *Mol Biol* **305**, 567-580, doi:10.1006/jmbi.2000.4315 (2001).
- 557 39 Vives, R. R. *et al.* A novel strategy for defining critical amino acid residues involved in
558 protein/glycosaminoglycan interactions. *J Biol Chem* **279**, 54327-54333,
559 doi:10.1074/jbc.M409760200 (2004).

- 560 40 Port, F., Chen, H. M., Lee, T. & Bullock, S. L. Optimized CRISPR/Cas tools for efficient
561 germline and somatic genome engineering in *Drosophila*. *Proc Natl Acad Sci U S A* **111**,
562 E2967-2976, doi:10.1073/pnas.1405500111 (2014).
- 563 41 Boulanger, A. *et al.* ftz-f1 and Hr39 opposing roles on EcR expression during *Drosophila*
564 mushroom body neuron remodeling. *Nat Neurosci* **14**, 37-44, doi:nn.2700 [pii]
565 10.1038/nn.2700 (2011).
- 566 42 Talbot, W. S., Swyryd, E. A. & Hogness, D. S. *Drosophila* tissues with different
567 metamorphic responses to ecdysone express different ecdysone receptor isoforms.
568 *Cell* **73**, 1323-1337 (1993).
- 569 43 Pfeiffer, B. D., Truman, J. W. & Rubin, G. M. Using translational enhancers to increase
570 transgene expression in *Drosophila*. *Proc Natl Acad Sci U S A* **109**, 6626-6631,
571 doi:10.1073/pnas.1204520109 (2012).
- 572 44 Hoover, D. M., Mizoue, L. S., Handel, T. M. & Lubkowski, J. The crystal structure of the
573 chemokine domain of fractalkine shows a novel quaternary arrangement. *J Biol Chem*
574 **275**, 23187-23193, doi:10.1074/jbc.M002584200 (2000).
- 575 45 McLaughlin, C. N., Perry-Richardson, J. J., Coutinho-Budd, J. C. & Broihier, H. T. Dying
576 Neurons Utilize Innate Immune Signaling to Prime Glia for Phagocytosis during
577 Development. *Dev Cell* **48**, 506-522 e506, doi:10.1016/j.devcel.2018.12.019 (2019).
- 578 46 Doherty, J. *et al.* PI3K signaling and Stat92E converge to modulate glial responsiveness
579 to axonal injury. *PLoS Biol* **12**, e1001985, doi:10.1371/journal.pbio.1001985 (2014).

580
581

582 **Acknowledgements**

583 We thank Amélie Babled, Pascal Carne and Dana Bis-Brewer for help in the EMS
584 mutagenesis, MB developmental studies and WGS analysis respectively, Oren Schuldiner for
585 discussions about the Orion expression and function. We thank Marc Freeman for *alrm-GAL4*
586 stock, Baeg Gyeong Hun for *10X-STAT92E-GFP* stock, the Bloomington *Drosophila* Stock
587 Center and VDRC for fly stocks, the *Drosophila* facility, BioCampus Montpellier, CNRS,
588 INSERM, Université de Montpellier, the imaging facility MRI, which is part of the UMS
589 BioCampus Montpellier and a member of the national infrastructure France-BioImaging,
590 supported by the French National Research Agency (ANR-10-INBS-04) for help in confocal
591 and image analysis and processing. We acknowledge BDGP, BestGene, GenScript and
592 Genewiz for cDNA clone, transgene service, gene synthesis and DNA sequencing, respectively.
593 The 1D4 anti-Fasciclin II hybridoma and the 8D12 anti-Repo monoclonal antibody developed
594 by Corey Goodman and the 8A1 anti-Draper monoclonal antibody developed by Mary Logan
595 were obtained from the Developmental Studies Hybridoma Bank, created by the NICHD of the
596 NIH and maintained at The University of Iowa, Department of Biology, Iowa City, IA 52242.

597 **Funding:** C.T. was supported by grants from the INSB at the CNRS and from the Fondation
598 pour la Recherche Médicale. Work in the laboratory of J.-M.D. was supported by the Centre

599 National de la Recherche Scientifique, the Association pour la Recherche sur le Cancer (grants
600 SFI20121205950 and PJA 20151203422) and the Fondation pour la Recherche Médicale
601 (Programme "EQUIPES FRM2016" project DEQ20160334870).

602

603 **Author contributions**

604 A.B. and J.-M.D. designed the project; A.B., C.T. and J.-M.D. performed the experiments;
605 A.B., S.Z., L.G.F., H.L.-J. and J.-M.D. analyzed the data; A.B. and J.-M.D. wrote the original
606 draft of the manuscript; A.B., L.G.F., H.L.-J. and J.-M.D. reviewed and edited the manuscript.

607

608 **Competing interests**

609 The authors declare no competing interests.

610

611 **Additional information**

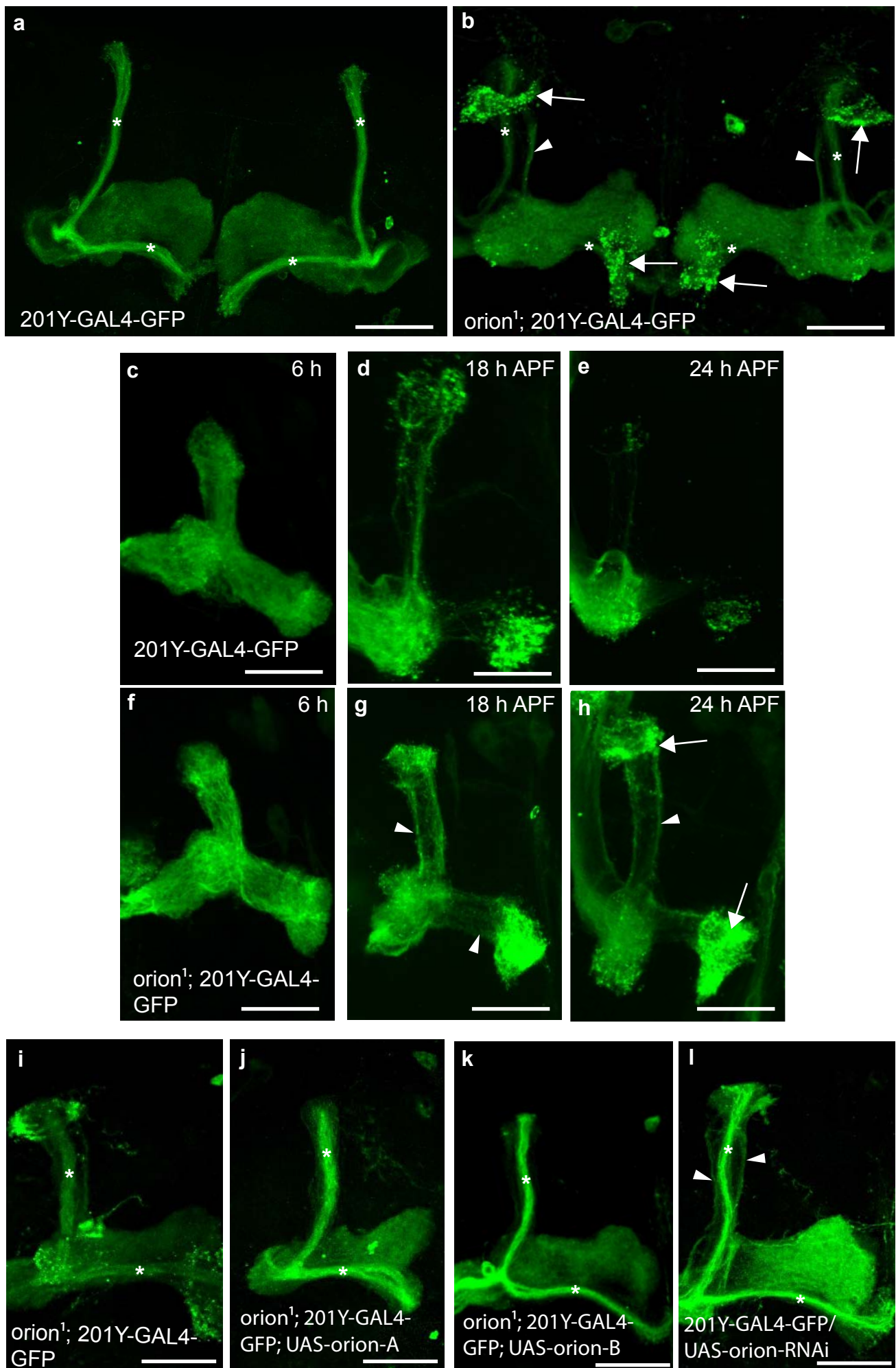
612 **Supplementary information:** Supplementary Fig. 1 to 10 and Supplementary list of fly strains

613

614

615

Fig. 1



616 **Fig. 1. The *orion* gene is necessary for MB remodeling.** **a-l**, γ neurons are visualized by the
617 expression of *201Y-GAL4* driven *UAS-mCD8-GFP* (green). In adults, this GAL4 line also
618 labels the $\alpha\beta$ -core axons shown here by asterisks. **a, b**, Adult γ axons in control (**a**) and *orion*¹
619 (**b**). Note the presence of unpruned γ axon bundles (arrowhead) and the high amount of
620 uncleared axonal debris (arrows) in *orion*¹ compared to wild-type ($n \geq 100$ MBs for control and
621 *orion*¹. See quantitation in Table I and Supplementary Fig. 2). **c-h**, γ axon development in wild-
622 type (**c-e**) and *orion*¹ (**f-h**) at 6 h, 18 h and 24 h APF as indicated. Unpruned axons (arrowhead)
623 in *orion*¹ are already apparent at 18 h APF (compare **g** with **d**) although no differences are
624 detected at 6 h APF (**c** and **f**). Note the presence of unpruned γ axons (arrowhead) and debris
625 (arrow) in *orion*¹ at 24 h APF ($n \geq 40$ MBs for each developmental stage). **i-k**, The adult *orion*¹
626 phenotype (**i**) is completely rescued by expression in MBs of *UAS-orion-A* ($n = 89$ MBs) (**j**) or
627 *UAS-orion-B* ($n = 387$ MBs) (**k**). **l**, *UAS-orion-RNAi* expression in MBs results in unpruned γ
628 axon phenotypes (arrowheads) ($n = 20$ MBs). Scale bars represent 40 μm . All the images are
629 composite confocal images. Genotypes are listed in Supplementary list of fly strains.
630

Table I

Presence of unpruned axons in \geq one-week-old adults

a

	MB	None	Weak	Strong
WT	25	25	0	0
Hr39	22	0	0	22
orion Δ C	22	0	22	0
orion1	20	0	20	0
orionRNAi	34	0	34	0
drpr Δ 5	22	20	2	0

Presence of axon debris in \geq one-week-old adults

b

	MB	None	Mild	Intermediary	Strong
WT	25	25	0	0	0
Hr39	22	22	0	0	0
orion Δ C	22	0	0	0	22
orion1	20	0	0	0	20
orionRNAi	34	34	0	0	0
drpr Δ 5	22	16	2	2	2

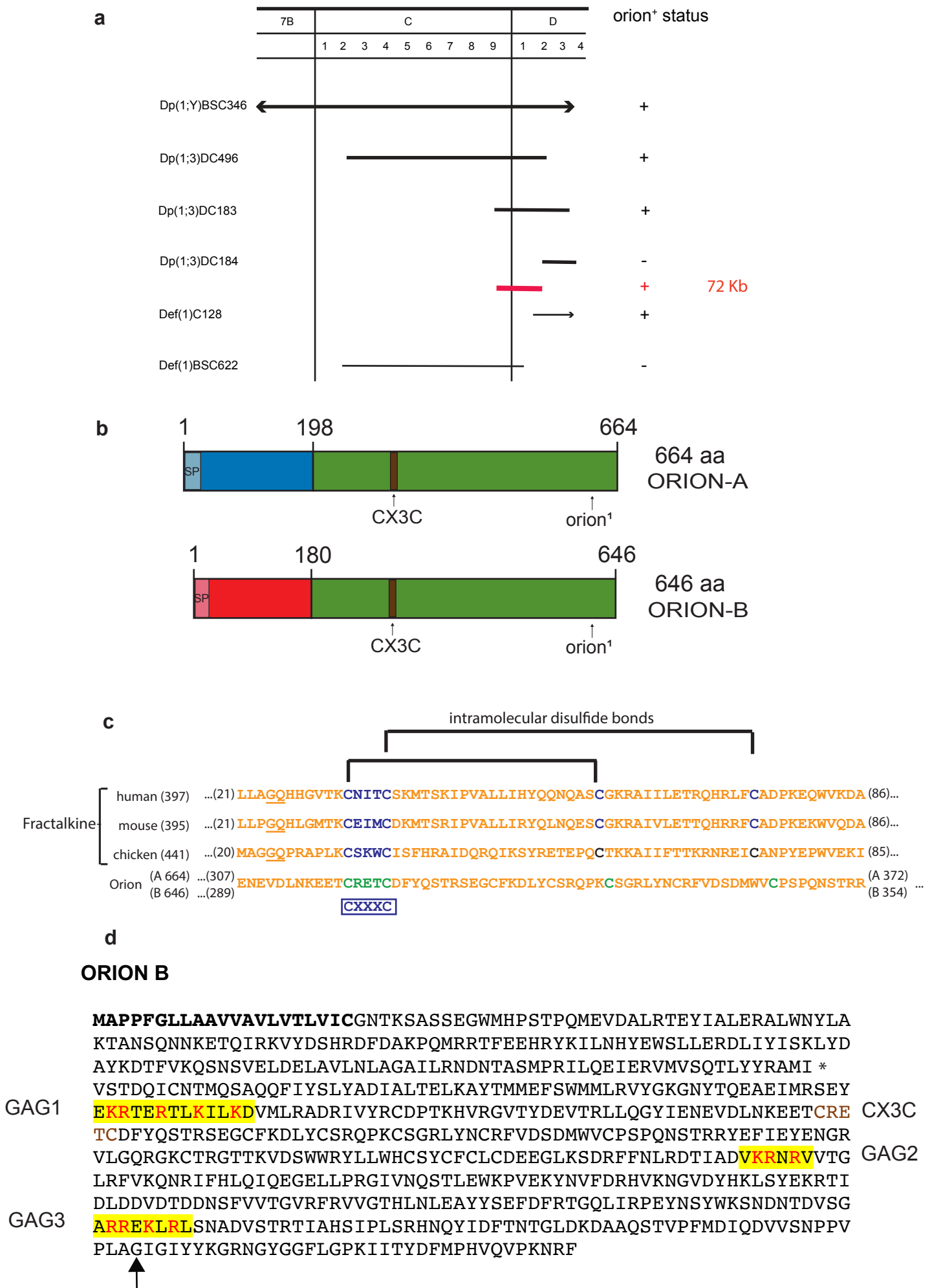
Presence of axon debris in \leq 2 h-old adults

c

	MB	Scattered dots	Mild	Intermediary	Strong
WT	10	10	0	0	0
orion Δ C	12	0	0	0	12
drpr Δ 5	73	40	11	4	18

631 **Table I. Unpruned axon and axon debris quantitation.** Genotypes are indicated on the left.
632 “MB“ indicates the number of mushroom bodies observed for each genotype. Unpruned axons
633 were ranked in three categories: “None” indicates the absence of unpruned γ axons, “Weak”
634 and “Strong” refer to different levels of the mutant pruning phenotype. Axon debris were ranked
635 in five categories: “None” indicates the absence of debris, “Scattered dots” means that some
636 individual debris can be observed. “Mild”, “Intermediate” and “Strong” refer to different levels
637 of debris (see Supplementary Fig. 2 and Methods). Full genotypes are listed in Supplementary
638 list of fly strains.
639

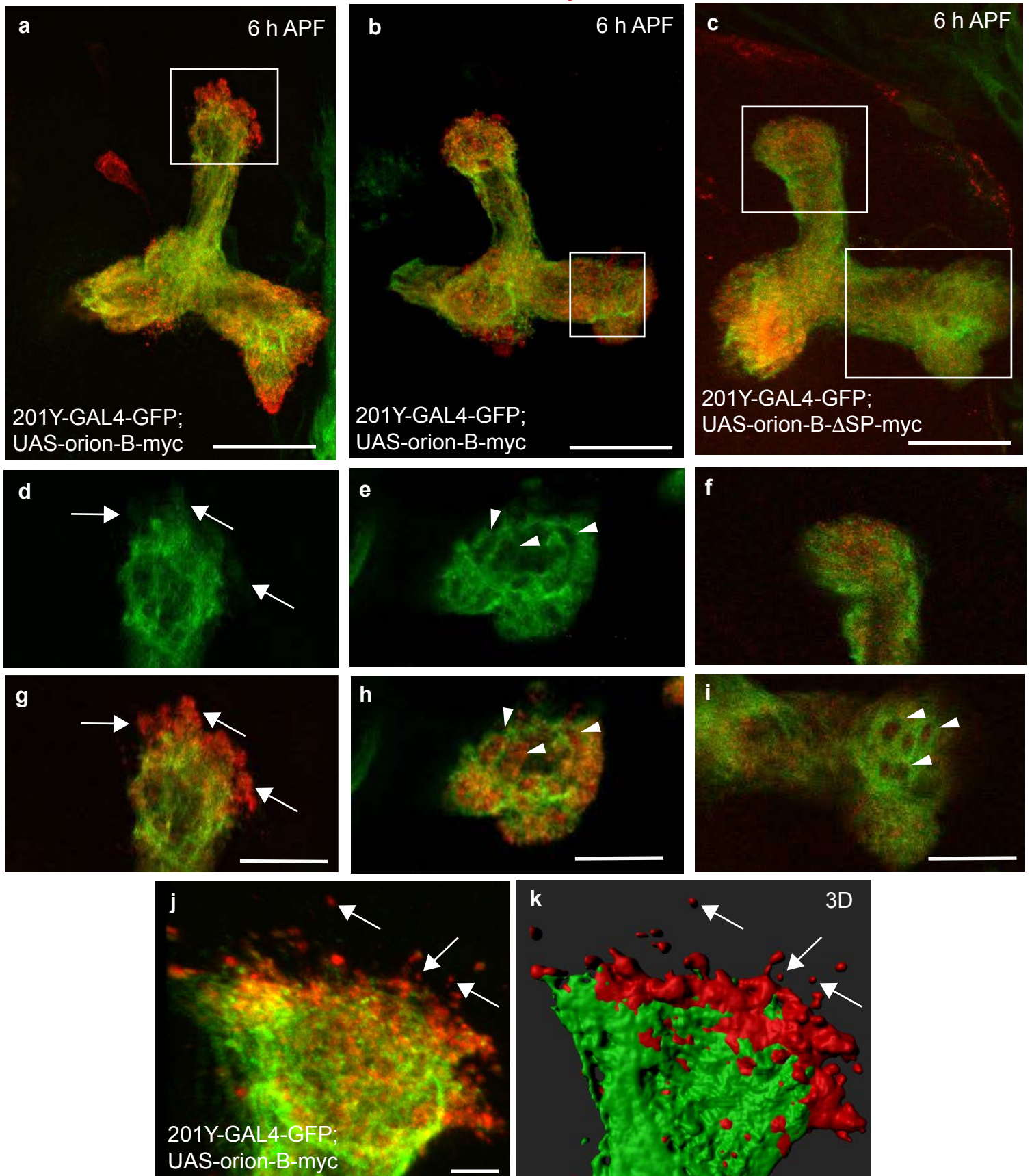
Fig. 2



640 **Fig. 2. The *orion* gene encodes for a CX₃C motif-containing protein.** **a**, Complementation
641 map of *orion* with the tested duplications and deficiencies in the 7B-7D region. Duplications
642 are drawn with a heavy line and deficiencies with a light line. If *orion*⁺ is present on the
643 chromosome carrying a duplication or deficiency it is indicated in the status column with a “+”;
644 and if it is not present it is marked “-“. The red line indicates the location of the 72 kb to which
645 *orion* is mapped based on the complementation results. **b**, Linear representation of the
646 polypeptide chain of the two Orion isoforms. Green represents the common region of the two
647 Orion proteins, blue is the specific N-terminal region of Orion-A and red the specific N-terminal
648 region of Orion-B. The signal peptide of Orion-A and Orion-B (SP) are colored in light blue or
649 light red, respectively. The CX₃C chemokine-motif as well as the location of the *orion*^l
650 mutation present in the common region of Orion-A and Orion-B are indicated. **c**, Amino acid
651 sequence lineups of human, mouse and chicken fractalkines with the common CX₃C-bearing
652 motif of the *Drosophila* Orion proteins is shown. The number in parenthesis after the species’
653 names indicate the total length of the protein. The underlined sequences in the fractalkine
654 sequences indicate the junctions at which their signal peptides are cleaved. The numbers at the
655 beginning and end of the sequence indicate the protein regions in the lineup. The CX₃C
656 (CXXXC) and conserved downstream cysteines in the fractalkine species are indicated in blue.
657 Fractalkine intramolecular disulfide bonds between conserved cysteines⁴⁴ are specified with
658 brackets. The CX₃C motif in the Orions and the downstream cysteines are indicated in green.
659 The Orion downstream cysteines are offset by one and two amino acids, respectively, from
660 those in fractalkine relative to the CX₃C motif cysteines. The Orions differ from fractalkine
661 by the inclusion of considerable extensions upstream to the CX₃C motif while the fractalkine
662 CX₃C motifs lie within 10 amino acids of the mature signal peptide-cleaved proteins. **d**, Orion-
663 B amino-acid sequence where the signal peptide is in bold, the three putative GAG binding
664 sites (GAG1, GAG2, GAG3) are highlighted in yellow, the basic residues involved in GAG
665 binding (R = Arg and K = Lys) are in red and the CX₃C site is in brown. An asterisk is located
666 at the end of the Orion-B specific amino-acid sequence/beginning of the common region. The
667 glycine (GGC) which is mutated to an aspartic acid (GAC) in *orion*^l is indicated by an arrow.
668

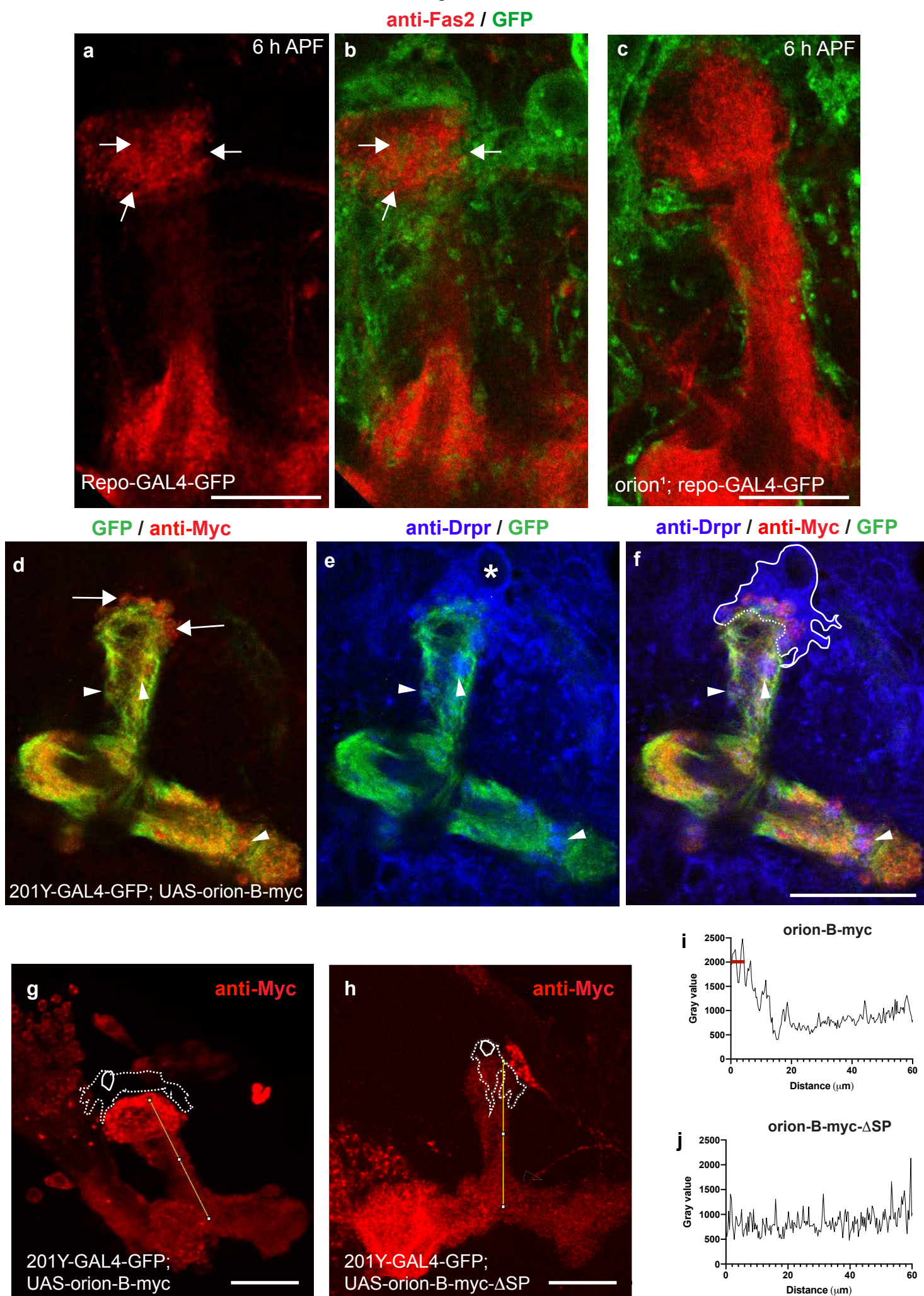
Fig. 3

GFP / anti-Myc



669 **Fig. 3. Orion is secreted by MB γ axons. a-k** 6 h APF γ axons are visualized by the expression
670 of *201Y-GAL4*-driven *UAS-mCD8-GFP* (green). **a, b, j, k**, γ axons expressing the wild-type
671 Orion-B-Myc protein (red) ($n \geq 10$ MBs). **c**, γ axons expressing the Orion-B-Myc protein
672 lacking the signal peptide (Δ SP) ($n = 9$ MBs). **a-c** are confocal Z-projections and **j** is a unique
673 confocal plane. **d, g**, higher magnification images of the region indicated by rectangle in **a**
674 showing a representative unique confocal plane. Note the presence of Myc-labelled Orion-B
675 outside of the γ axon bundle (arrows). **e, h**, higher magnification images of the region indicated
676 by rectangle in **b** showing a representative unique confocal plane. Note the presence of Myc-
677 labelled Orion-B inside of the hole-like structures present in the γ axon bundle (arrowheads). **f,**
678 **i**, higher magnification images of the vertical and medial γ lobes, respectively (rectangles in **c**).
679 Orion-B- Δ SP-Myc is not observed neither outside of the γ axons (**f**) nor in the hole-like
680 structures (arrowheads in **i**). **j, k** Presence of Myc-labelled Orion-B secreted proteins not
681 associated with GFP-labelled axon membranes can be observed outside of the γ axon bundle
682 (arrows). **k**, Three-dimensional surface-rendering (3D) of the confocal image. **j**, reveals close
683 apposition of GFP-labelled axons and Myc-labelled Orion and reveals Orion is present as small
684 extracellular globules. Scale bars represent 40 μm in **a-c**, 20 μm in **d-i** and 5 μm in **j, k**. Full
685 genotypes are listed in Supplementary list of fly strains.
686

Fig. 4



687 **Fig. 4. Orion is required for the infiltration of astrocytes into the MB γ bundle at 6 h APF.**

688 **a-c**, Single confocal planes of 6 h APF brains expressing *repo-GAL4*-driven *UAS-mCD8-GFP*
689 (green) in controls (**a, b**) and *orion¹* (**c**) focused on the MB dorsal lobe (n = 12 MBs controls
690 and n = 20 MBs *orion¹*). Anti-Fas2 staining (red) reveals spherical hole-like structures occupied
691 by glial processes infiltrating into the γ bundle (green, arrows) in wild-type (**a, b**) but not in
692 *orion¹* individuals (**c**). Scale bars are 20 μ m. **d-f**, A single confocal plane showing the
693 expression of *201Y-GAL4* driven *UAS-mCD8-GFP* (green, **d-f**) and Orion-B-Myc (red, **d, f**) in
694 6 h APF MB. Anti-Drpr antibody (blue) was used to visualize the glial cells (blue, **e, f**). **d**,
695 displays Orion-B-Myc expression outside of the axons at the top of the vertical γ bundle
696 (arrows) as well as in hole-like structures (arrowheads). **e**, displays an astrocyte positioned at
697 the top of the γ bundle (asterisk in its nuclei) as well as several astrocyte processes occupying
698 hole-like structures (arrowheads). Note the co-localization of Orion-B-Myc and glia processes
699 in the hole-like structures (arrowheads in **f**). The astrocyte cell membrane (continuous line) and
700 the membrane contacting the tip of the γ bundle (dotted line), where phagocytosis is taking
701 place, based on our interpretation of the astrocyte limits according to the green and the blue
702 channels for GFP and Drpr, respectively, are indicated in **f**. Scale bar is 40 μ m. **g, h**,
703 Representative images to illustrate how the quantitation of Orion-B-Myc expression (red), **g**,
704 and Orion-B- Δ SP-Myc, **h**, driven by *201Y-GAL4* in a traced 60 μ m line contained in a γ axon
705 vertical bundle was performed. The position of an astrocyte (dotted line), labeled by anti-Drpr
706 staining (not shown), and its nucleus (solid circle) are indicated. **i, j** Representative plotted
707 intensity profiles of Orion expression (gray value) in Orion-B-Myc- (**i**) or Orion-B- Δ SP-Myc-
708 expressing MBs (**j**), according to the distance from the tips (0 μ m) to the bottoms (60 μ m) of
709 vertical γ bundles. The highest peaks are always located at less than 7 μ m distance to the tip of
710 the vertical bundle (red bar) when Orion-B-Myc is expressed (n = 10) although this was never
711 the case (n = 9) when secretion-deficient Orion-B- Δ SP-Myc expression was quantified. Scale
712 bar in **g** and **h** are 30 μ m. Full genotypes are listed in Supplementary list of fly strains.

713

714

715

716

717

718

719

720

721 **Supplementary Materials for**

722

723 **Axon-secreted chemokine-like Orion is a signal for astrocyte infiltration**
724 **during neuronal remodeling**

725

726 Ana Boulanger^{1*}, Camille Thinat¹, Stephan Züchner², Lee G. Fradkin³, Hugues Lortat-Jacob⁴
727 and Jean-Maurice Dura^{1*}

728

729

730 *e-mail: ana.boulanger@igh.cnrs.fr; jean-maurice.dura@igh.cnrs.fr

731

732

733

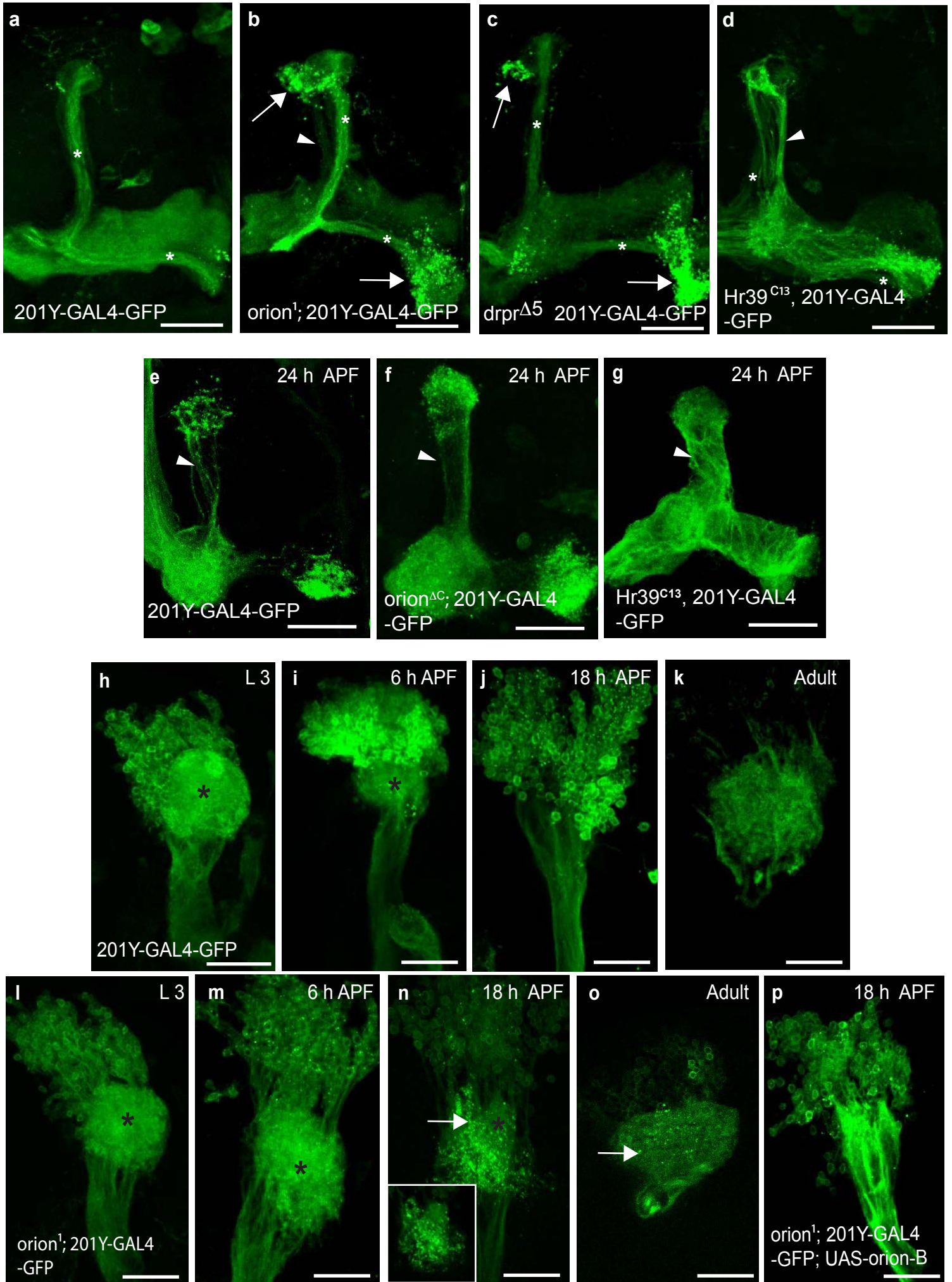
734 Supplementary Fig. 1 to 10

735

Supplementary list of fly strains

736

Supplementary Fig. 1



737 **Supplementary Fig. 1. The *orion* gene is necessary for γ axon and dendritic remodeling.**

738 **a-d**, Expression of *201Y-GAL4*-driven *UAS-mCD8-GFP* (green) in adult MB γ axons. In adults,
739 this GAL4 line also labels the $\alpha\beta$ -core axons indicated here by asterisks. Wild-type (**a**), *orion^l*
740 (**b**), *draper ^{Δ 5}* (**c**) and *Hr39^{C13}* (**d**) (n = 22, 26, 30 and 4 MBs). The glial phagocytic receptor
741 *Drpr* is required for MB remodeling¹³. Note the significant similarity between the *orion^l* and
742 *draper ^{Δ 5}* phenotypes with respect to the distribution and the amount of axonal debris remaining
743 (arrows in **b** and **c**); they differ by the presence of unpruned γ axons only in *orion^l* (arrowhead
744 in **b**; see also Fig. 1b). In addition, the *draper ^{Δ 5}* phenotype is observed only in very young flies
745¹³. In contrast, the *orion^l* phenotype persists throughout adult life at least up to one month old
746 in *orion^l* males. Expression of *Hr39* in γ neurons results in only unpruned γ axons (arrowhead)
747 without debris (**d**). In this case, the pruning process is completely blocked due to the *EcR-B1*
748 down-regulation by *Hr39* thus precluding the generation of axon debris⁴¹. **e-g**, Expression of
749 *201Y-GAL4*-driven *UAS-mCD8-GFP* (green) in γ neuron axons at 24 h APF. γ axon
750 development was observed in wild-type (**e**), *orion^{AC}* (**f**) and *Hr39^{C13}* (**g**) as indicated. In wild-
751 type (**e**), only some scattered γ axons are still unpruned (arrowhead). Additional unpruned
752 fascicles of axons (arrowhead) are apparent in *orion^{AC}* (compare **f** with **e**). Note the massive
753 presence of unpruned γ axons (arrowhead) in *Hr39^{C13}* (**g**), where the γ axon-intrinsic
754 fragmentation process is blocked. However, since the axon-intrinsic fragmentation process is
755 still functional in *orion^{AC}*, the number of these unpruned axons is much lower than in *Hr39^{C13}*
756 (n \geq 10 MBs for each developmental stage). **h-p**, Expression of *201Y-GAL4*-driven *UAS-*
757 *mCD8-GFP* (green) in γ neuron dendrites (black asterisks) during development. Wild-type
758 control (**h-k**) and *orion^l* (**l-p**) γ dendrites are compared at L3, 6 h APF, 18 h APF and adult as
759 indicated. Note the presence of intact larval γ dendrites in *orion^l* (asterisk in **n** compared to
760 wild-type (**j**) at 18 h APF and the persistence of dendrite debris in *orion^l* at 18 h APF (arrow in
761 **n** as well as in adult (arrow in **o**). A confocal plane of a dendrite region containing larval
762 dendrite debris (brilliant dots) is enclosed by a rectangle in **n**. **p**, The *orion^l* unpruned dendritic
763 phenotype is rescued by expression of *UAS-orion-B* at 18 h APF. All the pictures are confocal
764 Z-projections (n is \geq 8 for each developmental stage). Scale bars are 40 μ m. Genotypes are
765 listed in Supplementary list of fly strains.

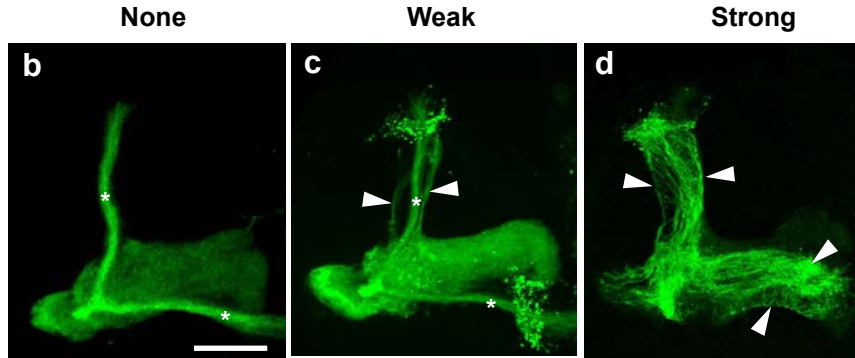
766

Supplementary Fig. 2

Presence of unpruned axons in \geq one-week-old adults

a

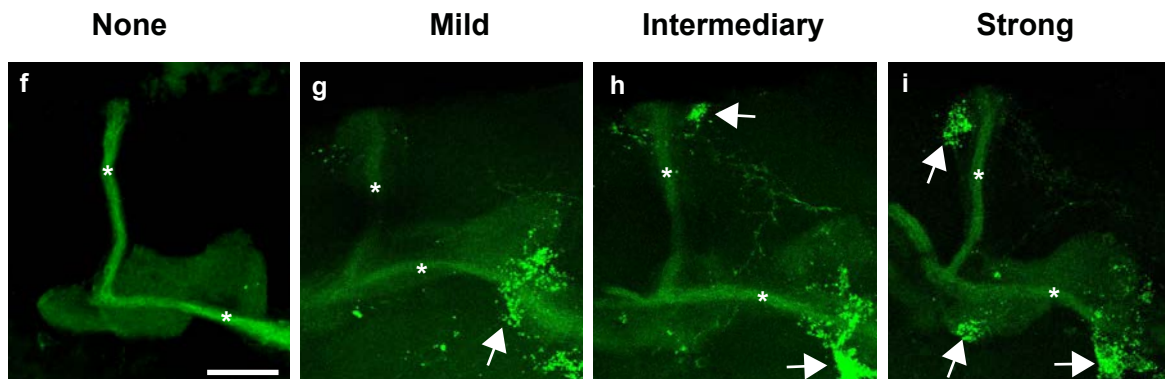
	MB	None	Weak	Strong
WT	25	25	0	0
Hr39	22	0	0	22
orion Δ C	22	0	22	0
orion1	20	0	20	0
orionRNAi	34	0	34	0
drpr Δ 5	22	20	2	0



Presence of axon debris in \geq one-week-old adults

e

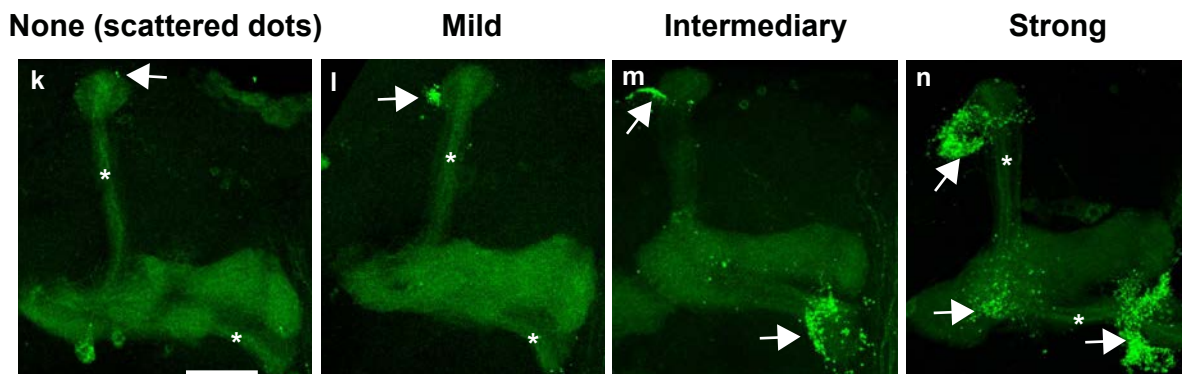
	MB	None	Mild	Intermediary	Strong
WT	25	25	0	0	0
Hr39	22	0	0	0	0
orion Δ C	22	0	0	0	22
orion1	20	0	0	0	20
orionRNAi	34	34	0	0	0
drpr Δ 5	22	16	2	2	2



Presence of axon debris in \leq 2 h-old adults

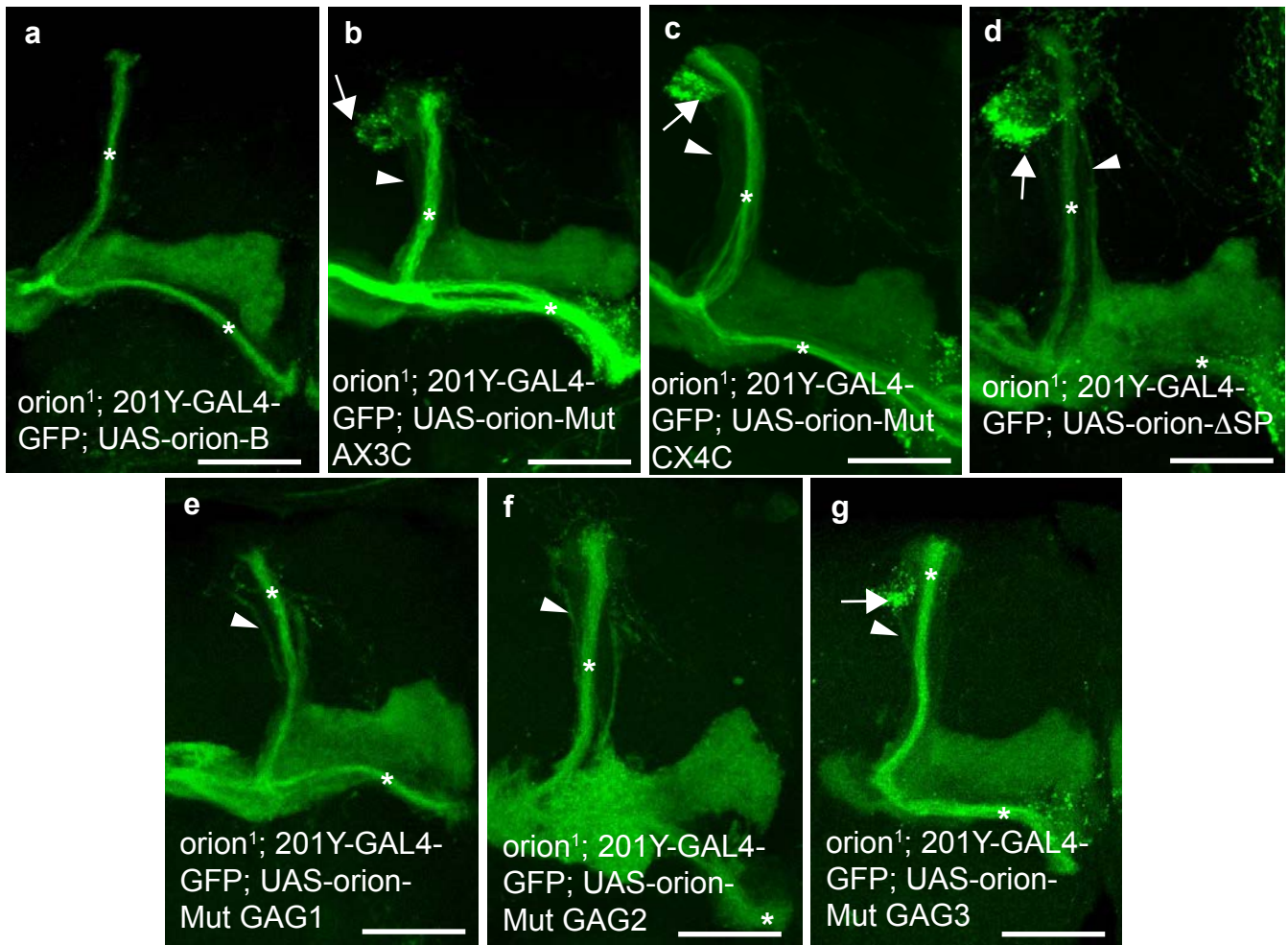
j

	MB	Scattered dots	Mild	Intermediary	Strong
WT	10	10	0	0	0
orion Δ C	12	0	0	0	12
drpr Δ 5	73	40	11	4	18



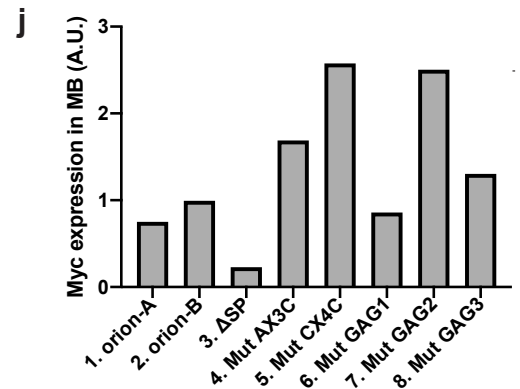
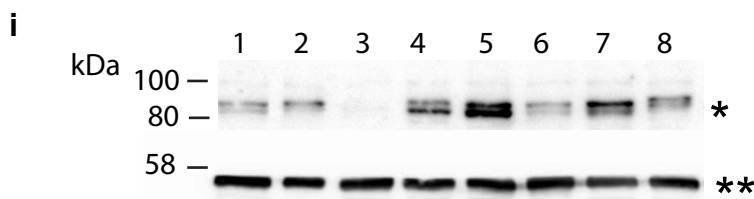
767 **Supplementary Fig. 2. Unpruned axons and axon debris phenotypes.** Tables **a**, **e** and **j** show
768 quantitation of the unpruned axon (**a**) and axon debris (**e**, **j**) and are described in Table I. γ
769 neurons are visualized by the expression of *201Y-GAL4* driven *UAS-mCD8-GFP* (green). In
770 adults, this *GAL4* line also labels the $\alpha\beta$ -core axons indicated here by asterisks. Unpruned
771 axons are labeled by arrowheads in **c** (“Weak”) and in **d** (“Strong”). Axon debris are ranked as
772 “Scattered dots” (**k**), “Mild” (**g**, **l**), “Intermediate” (**h**, **m**) and “Strong” (**i**, **n**) and are labelled
773 by arrows in **g-n**. These dots likely correspond to yet uncleared axon debris (**j**, **k**). Scale bars
774 are 30 μm . Genotypes are listed in Supplementary list of fly strains.
775

Supplementary Fig.3



h

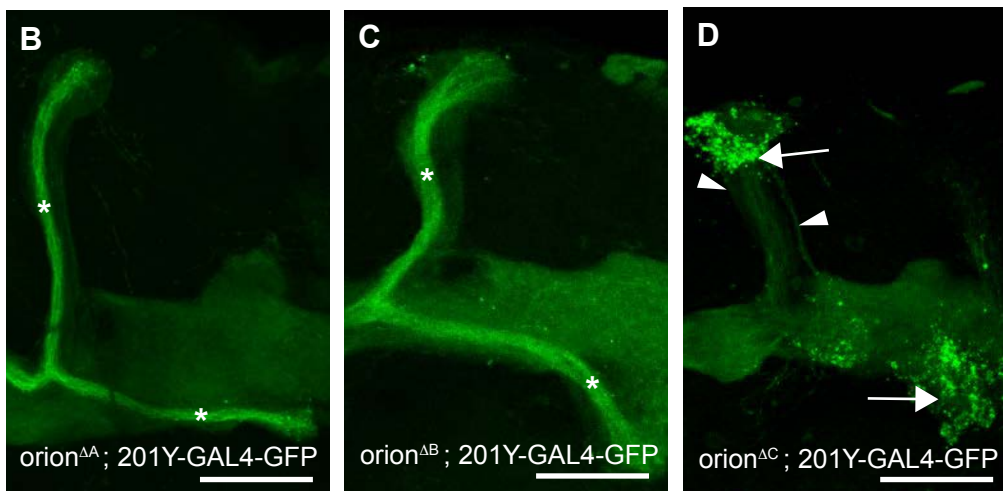
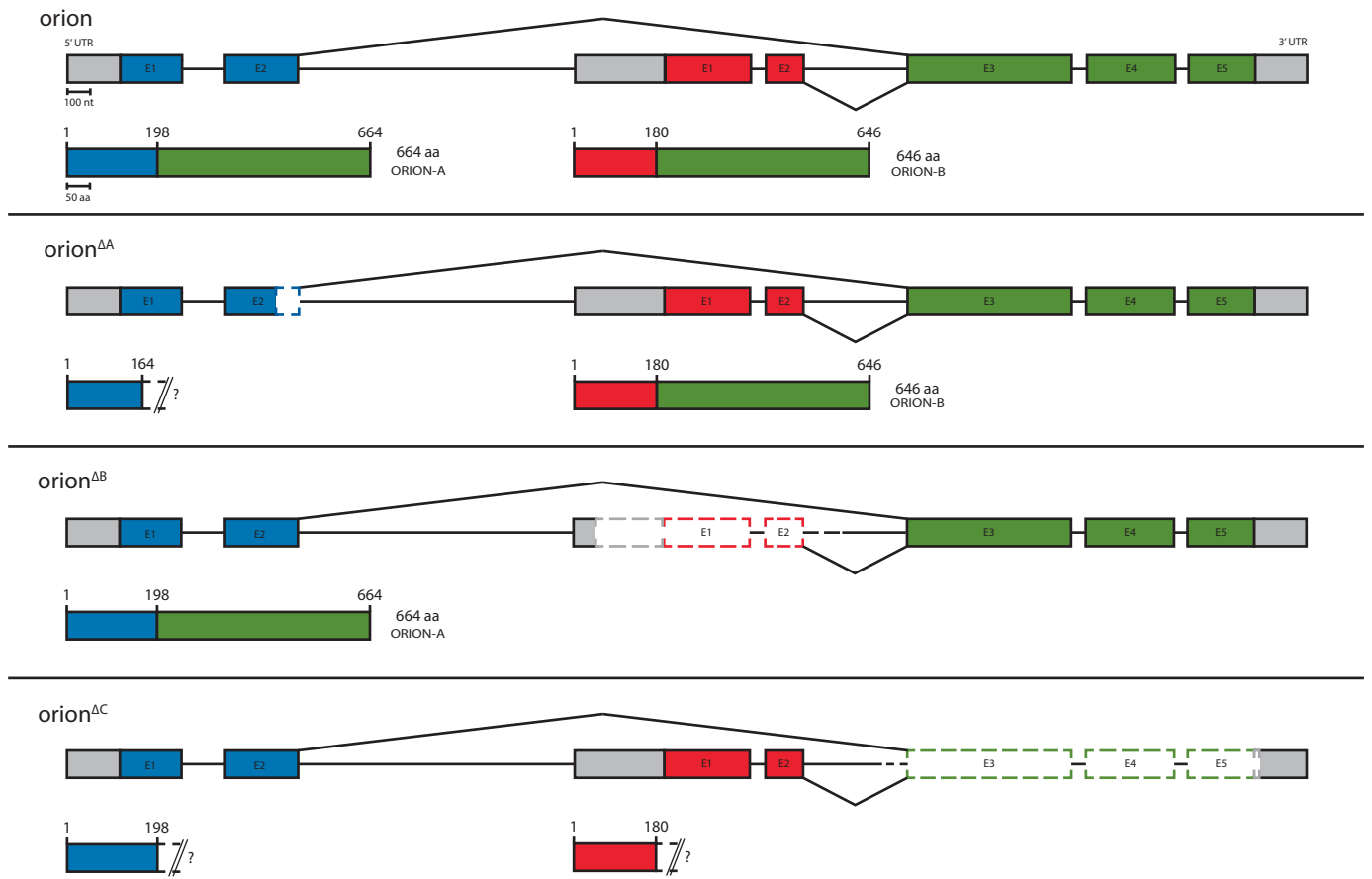
	MB	UP	Debris	WT
control	100	0	0	100
orion1	100	100	100	0
orion1 + orion-B WT	387	0	0	387
orion1 + ΔSP	27	27	27	0
orion1 + AX3C	20	20	20	0
orion1 + CX4C	20	20	20	0
orion1 + GAG1	106	46	0	60
orion1 + GAG2	122	52	0	70
orion1 + GAG3	118	112	112	6
orion-RNAi	34	34	0	0
orion-RNAi + EcRB1	26	2	0	24
orion-RNAi + control	20	20	0	0



776 **Supplementary Fig. 3. The CX₃C motif, the GAGs sites and the SP domain are required**
777 **for the Orion pruning function. a-g**, The expression of *201Y-GAL4* driven *UAS-mCD8-GFP*
778 (green) is shown in adult MBs in which expression of wild-type *UAS-orion-B* (**a**) (n = 387
779 MBs) or *UAS-orion-B* containing different mutations (Mut, **b-g**) was induced in *orion¹*. *UAS-*
780 *orion-B* contains each of the following mutations: at the CX₃C site (AX₃C in **b**, n = 20 MBs;
781 CX₄C in **c**, n = 20 MBs), absence of signal peptide (Δ SP in **d**, n = 27 MBs), at the GAG1 site
782 (EKRTERTLKILKD into EAATEATLAILAD in **e**, n = 106 MBs), at the GAG2 site
783 (VKRNRV into VAANAV in **f**, n = 122 MBs), at the GAG3 site (ARREKLRL into
784 AAAEALAL in **g**, n = 118 MBs). Unpruned γ axons are labelled by arrowheads, uncleared
785 debris are labelled by arrows and $\alpha\beta$ core axons are labeled by asterisks. Note that debris are
786 absent in **e** and **f**. Scale bars are 40 μ m. **h**, Quantitation of the phenotypes are shown. MB: total
787 number of MBs analyzed; UP: number of MBs containing unpruned γ axons; Debris: number
788 of MBs containing uncleared debris; WT: number of wild-type looking MBs. Genotypes are
789 listed in Supplementary list of fly strains. **i**, Western blot, incubated with an anti-Myc antibody,
790 displaying the Orion-Myc expression levels (single asterisk) produced by the different *UAS-*
791 *orion-myc* constructs driven by *201Y-GAL4* and the tubulin levels in each genotype (double
792 asterisk) as a control. Proteins were extracted from L3 brains. Lane 1: *orion-A*; lane 2: *orion-*
793 *B*; lane 3: *orion-B- Δ SP*; lane 4: *orion-B-Mut AX₃C*; line 5: *orion-B-Mut CX₄C*; line 6: *orion-*
794 *B-Mut GAG1*; lane 7: *orion-B-Mut GAG2*; lane 8: *orion-B-Mut GAG3*. **j**, Orion-Myc band
795 expression levels are shown in arbitrary units (A.U.) which are calculated as a ratio of the Myc
796 level to the loading control tubulin level for each genotype. Note that all of the proteins are
797 expressed at similar or higher levels relative to Orion-B except Orion- Δ SP whose expression is
798 lower likely due to protein destabilization resulting from the lack of the signal peptide.
799

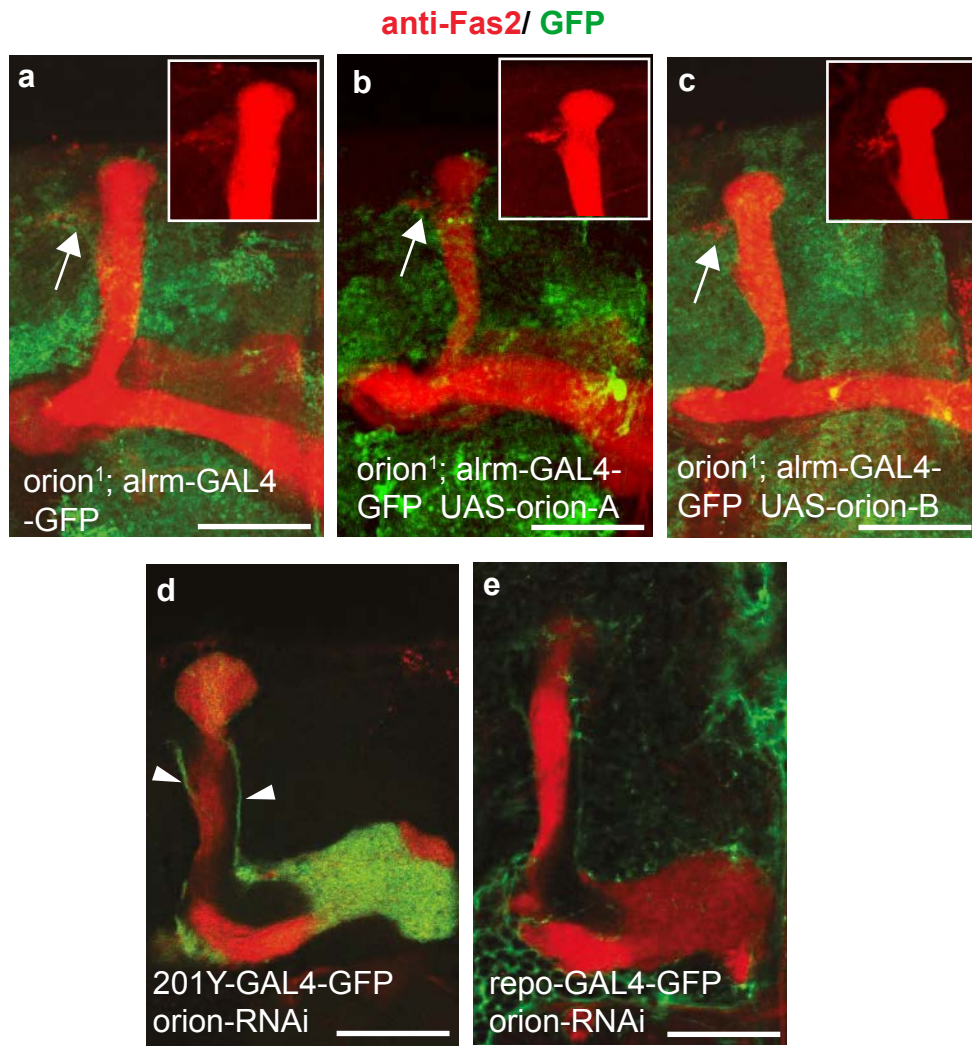
Supplementary Fig.4

A



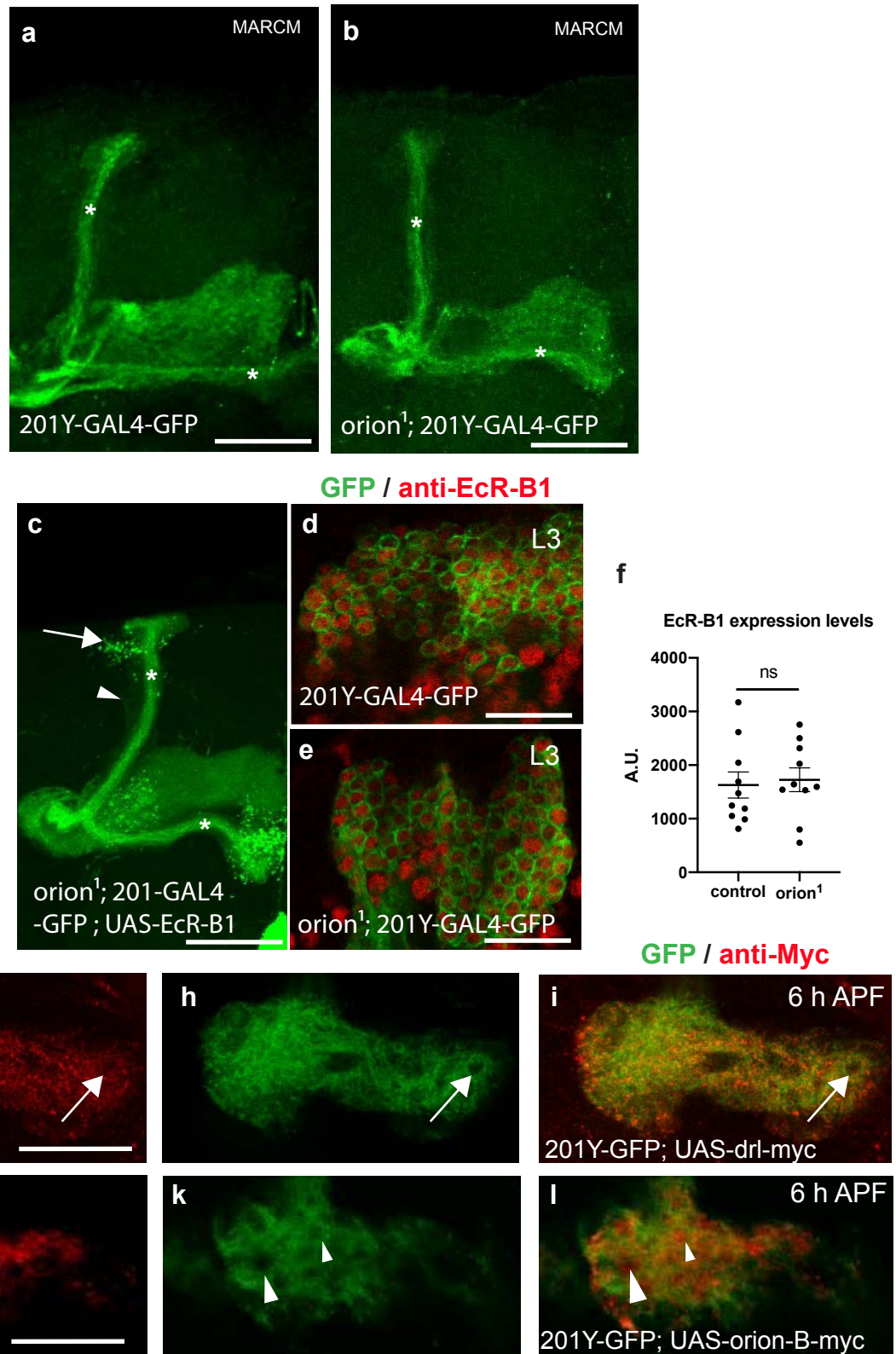
800 **Supplementary Fig. 4. Deletion of the common region of *orion* induces a γ axon pruning**
801 **phenotype.** The *orion* gene (CG2206) lies within the large intron of *Ubr3* and is referenced as
802 *l(1)G0193* although the lethality is clearly not due to the lack of *orion* function (see text) but
803 likely to some splicing defect of the *Ubr3* mRNA induced by the insertion of transposable
804 elements. **a**, Schematic representation of *orion* genomic DNA and its two Orion isoforms in
805 wild-type and in the three different CRISPR induced *orion* deletions (ΔA , ΔB and ΔC) and their
806 corresponding Orion isoforms. **b-d**, Confocal Z-projections of adult MB are revealed by *201Y-*
807 *GAL4*-driven *UAS-mCD8-GFP* expression (green) in the three *orion* CRISPR mutants: *orion* ^{ΔA} ,
808 *orion* ^{ΔB} and *orion* ^{ΔC} (n = 87, 70 and 98 MBs respectively). Only *orion* ^{ΔC} displays an unpruned
809 γ axon mutant phenotype characterized by unfragmented γ axons (arrowhead) and uncleared
810 debris (arrow). $\alpha\beta$ core axons are labeled by asterisks in **b** and **c** where they are clearly
811 discernible. Scale bars are 40 μ m. Genotypes are listed in Supplementary list of fly strains.
812
813

Supplementary Fig.5



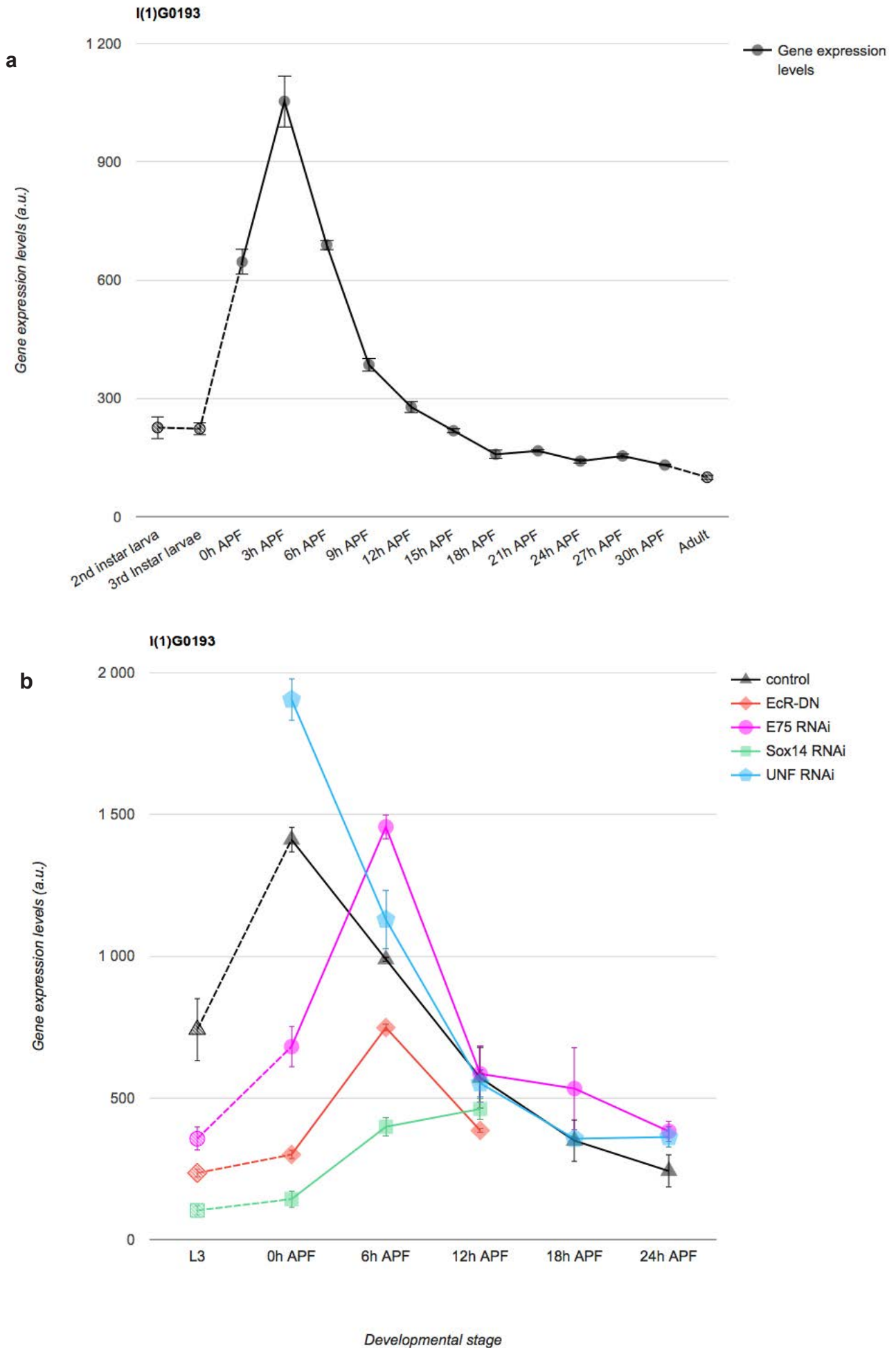
814 **Supplementary Fig. 5. Expression of Orion in glia does not rescue the *orion*¹ pruning**
815 **defect and downregulating Orion expression in wild-type glia does not affect pruning. a-**
816 **c,** Confocal Z-projections showing merged *alm-GAL4*-driven *UAS-mCD8-GFP* (green) and
817 anti-Fas2 staining (red) in *orion*¹ adult MBs. Expression of *orion-A* (b) or *orion-B* (c) in
818 astrocytes (*alm-GAL4*) does not rescue the *orion*¹ mutant phenotype. A rectangle containing
819 anti-Fas2 staining (red) is shown in a-c. Arrows point to unpruned γ axons and debris labelled
820 by anti-Fas2 (a-c). d, Confocal plane showing *201Y-GAL4*-driven *UAS-mCD8-GFP* (green)
821 and anti-Fas2 staining (red) in adult MBs. Expression of an *UAS-orion-RNAi* in MB neurons
822 results in an unpruned γ axon phenotype (arrowheads). e, Confocal plane showing *repo-GAL4*-
823 driven *UAS-mCD8-GFP* (green) and anti-Fas2 staining (red) in adult MBs. Expression of *orion*-
824 RNAi in glia does not result in unpruned γ axon phenotypes. Scale bars are 40 μ m and number
825 of MBs is ≥ 20 (a, n = 20; b, n = 20; c, n = 30; d, n = 20; e, n = 36 MBs). Genotypes are listed
826 in Supplementary list of fly strains.
827

Supplementary Fig.6



828 **Supplementary Fig. 6. Orion is a secreted protein with a non-cell-autonomous function in**
829 **γ axons. a-l**, The expression of *201Y-GAL4* driven *UAS-GFP* (green) reveals γ neurons. In adult
830 (a-c), L3 (d, e) and 6 h APF (g-l). a, b, MARCM neuroblast clones displaying wild-type γ axon
831 pruning are shown. A wild-type control (a) and an *orion*¹ (b) (n = 20 wild-type and 30 *orion*¹
832 neuroblast clones). c, *EcR-B1* expression in *orion*¹ γ neurons does not rescue the *orion*¹
833 phenotype. Note the presence of γ remnant debris (arrow) and unpruned axons (arrowhead) (n
834 = 40 MBs). d, e, Mushroom body cell body region showing ECR-B1 expression (red staining)
835 in wild-type (d) and *orion*¹ (e). f, Quantitation of EcR-B1 signal in γ neuron cell bodies in
836 arbitrary units (A.U.) reveals no significant differences between control and *orion*¹ (n = 10 MBs
837 for control and for *orion*¹; p = 0.67 (Mann-Whitney *U* test)). These interaction analyses support
838 *orion* being genetically downstream of *EcR-B1*. g-l, Expression of the transmembrane receptor
839 *drl-myc* (g-i, n = 10) and *orion-B-myc* (j-l, n = 10) in MBs. Red represents anti-myc staining.
840 Drl-myc staining is absent in hole-like structures (arrows in g-i). However secreted Orion-myc
841 is present in these structures (arrowheads in j-l). Images are confocal Z-projections, except for
842 g-l which are confocal planes. Scale bars are 40 μ m in a-c and g-l and 20 μ m in d and e.
843 Genotypes are listed in Supplementary list of fly strains.

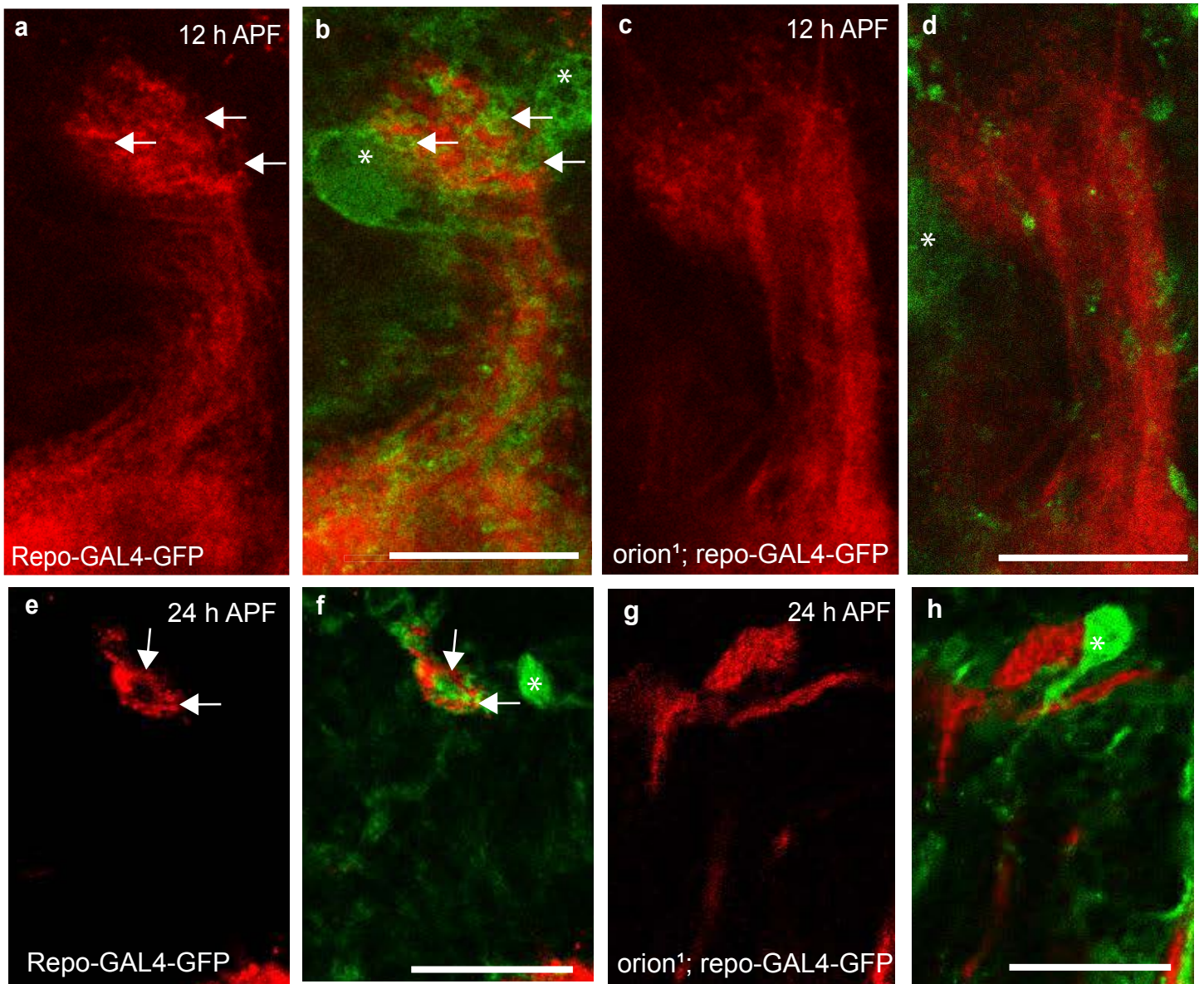
Supplementary Fig.7



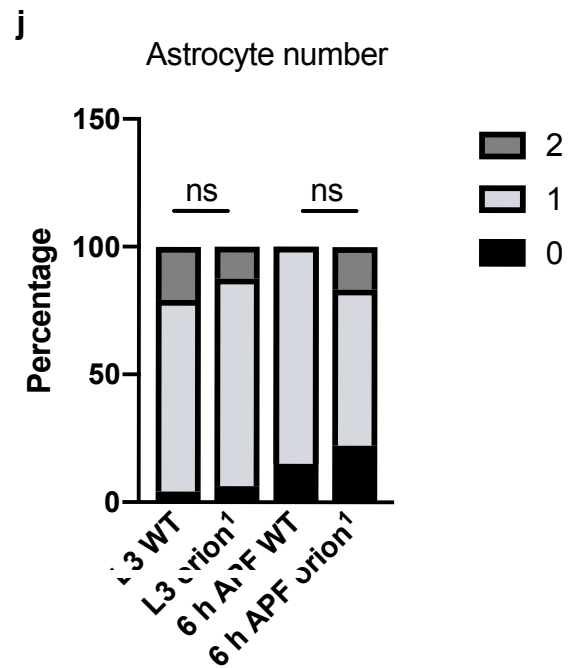
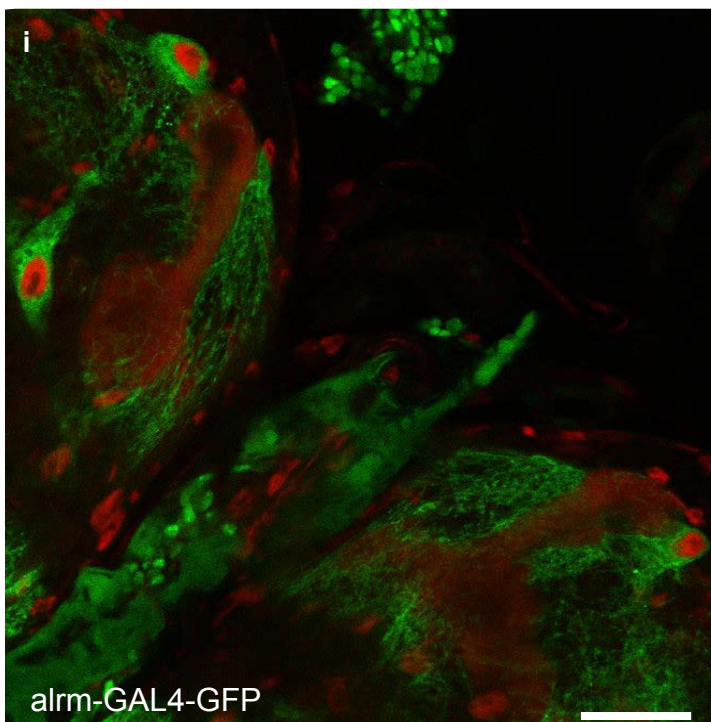
844 **Supplementary Fig. 7. *orion* mRNA is expressed at the time of pruning in γ neurons and**
845 **its expression is EcR-B1 regulated. a, b, Data showing *orion* mRNA γ neuron-expression**
846 **levels in arbitrary units (a.u.) during development in wild-type (a) and in different mutant**
847 **backgrounds (b), downloaded from Oren Schuldiner's laboratory's public web site**
848 **(<http://www.weizmann.ac.il/mcb/Schuldiner/resources>)²⁴. Note that the peak of expression of**
849 ***orion* is at 3 h APF which is the timepoint at which pruning initiates (a). We also note that just**
850 **before and during the pruning process (0-6 h APF) *orion* mRNA expression (black line in b) is**
851 **regulated by *EcR-B1* and *Sox14*.**
852

Supplementary Fig.8

anti-Fas2 / GFP



anti-Fas2 / anti-REPO / GFP

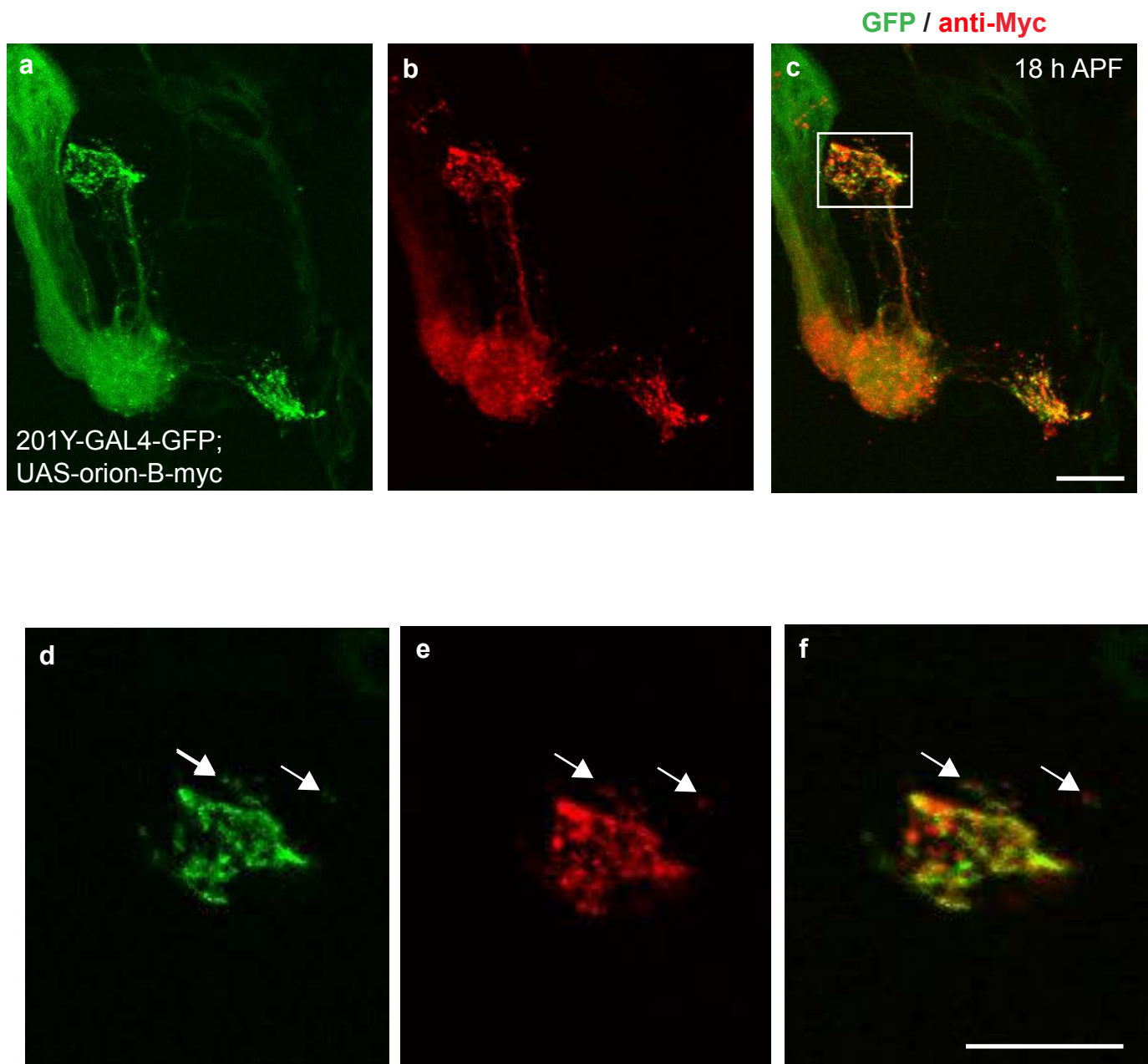


853 **Supplementary Fig. 8. Orion is required for the infiltration of astrocytes into the MB γ**
854 **bundle during development and its mutation does not alter the number of astrocytes**
855 **surrounding the γ axons.**

856 **a-h**, Confocal Z-projections of 12 h and 24 h APF brains expressing *repo-GAL4*-driven *UAS-*
857 *mCD8-GFP* (green) in controls (**a, b** for 12 h APF and **e, f** for 24 h APF) and *orion¹* (**c, d** for
858 12 h APF and **g, h** for 24 h APF) focused on the MB dorsal lobe (n = 10 control MBs and n =
859 10 *orion¹* MBs). Anti-Fas2 staining (red) reveals spherical hole-like structures occupied by glial
860 processes infiltrating into the γ bundle (green, arrows) in wild-type (**a, b** and **e, f**) but not in
861 *orion¹* individuals (**c, d** and **g, h**). Note the significant infiltration of the γ bundle by two
862 astrocytes in **b** (asterisk) and the absence of axon bundle infiltration by a closely apposed
863 astrocyte in **d** (asterisk). Nevertheless, the global aspect of the γ bundle where the fragmentation
864 is taking place looks similar in wild-type and mutant at 12 h APF. This suggests that, in *orion*
865 mutant, fragmenting γ axons are not actively being engulfed by astrocytes. Scale bars are 20
866 μm . **i**, Confocal Z-projection showing *UAS-mCD8-GFP* expression (green) in astrocytes driven
867 by *alrm-GAL4* at L3. Red shows both glial cell nuclei labelled by an anti-Repo antibody and
868 MBs labelled by anti-Fas2. Scale bars are 40 μm . **j**, Percentage of astrocytes surrounding the γ
869 vertical lobe at L3 and at 6 h APF in wild-type and *orion¹* (for L3, n = 24 wild-type MBs and n
870 = 16 *orion¹* MBs; for 6 h APF, n = 20 wild-type MBs and n = 18 *orion¹* MBs). No statistically-
871 significant differences were observed between the two groups (Fisher's exact test p = 0.84 for
872 L3 and p = 0.12 for 6 h APF). Scale bar is 30 μm . Genotypes are listed in Supplementary list
873 of fly strains.

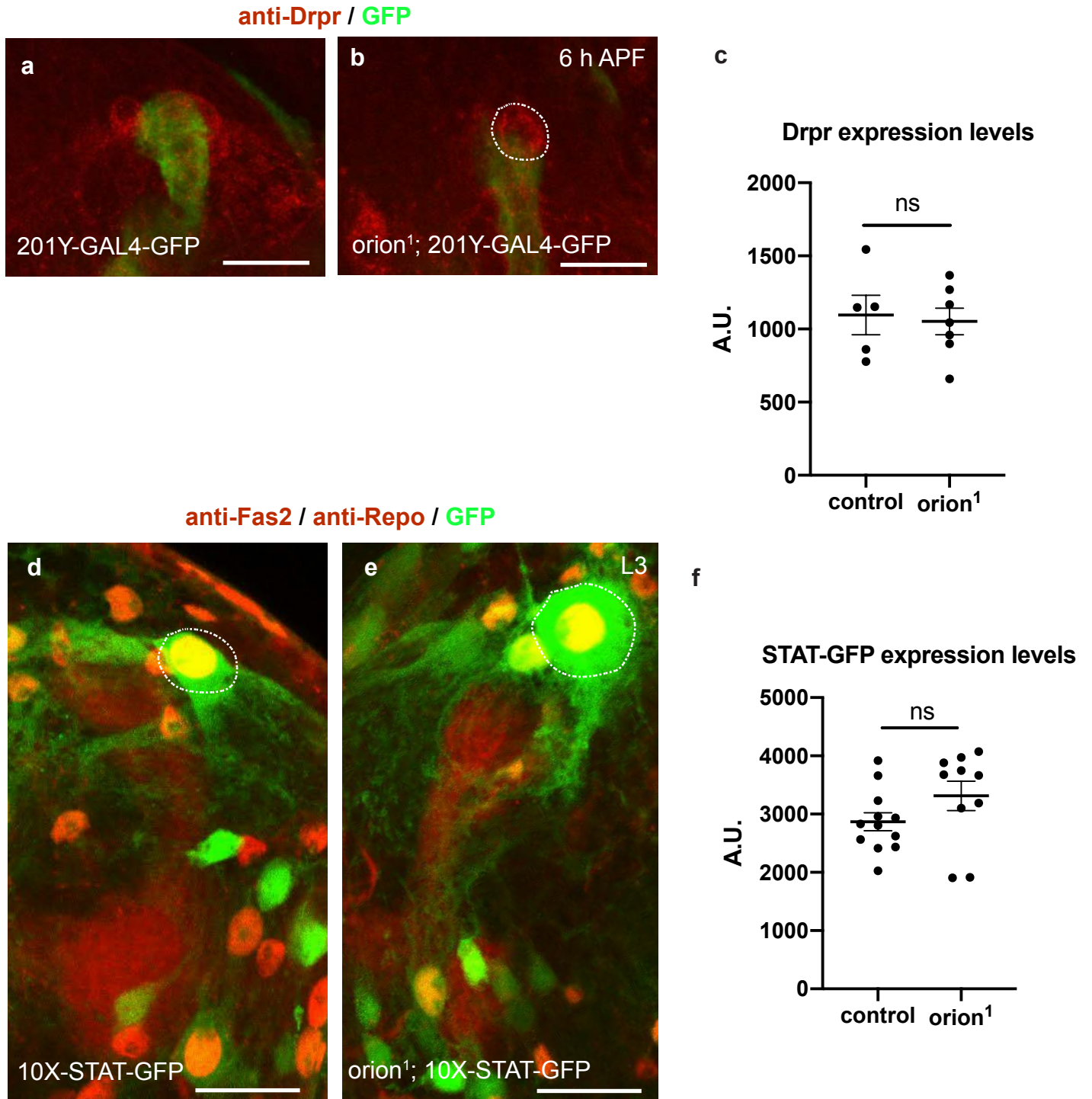
874
875
876
877
878

Supplementary Fig.9



879 **Supplementary Fig. 9. Orion is associated with membranes. a-c**, Expression of *UAS-mCD8-*
880 *GFP* (green) and *UAS-orion-B-myc* (red) under the control of *201Y-GAL4* is shown in 18 h
881 APF γ neurons (n = 6). **d-f**, (confocal planes) are higher magnifications of the **a-c** (confocal Z-
882 projections) regions enclosed by rectangles. Some debris staining for both GFP and Orion-Myc
883 is labelled by arrows. Scale bars are 20 μ m. Genotypes are listed in Supplementary list of fly
884 strains.

Supplementary Fig.10



885 **Supplementary Fig. 10. *orion*¹ mutants display wild-type levels of Drpr protein expression**
886 **and wild-type activity of the *drpr* transcriptional regulator STAT92E.** Since *drpr*
887 expression is regulated by known axon degeneration cues^{30,45} and the *drpr*^{Δ5} and *orion*¹ alleles
888 display mutant phenotypes that share some features (Supplementary Fig.1), we analyzed Drpr
889 expression in wild-type and *orion*¹. **a-c**, Expression of Drpr (red) in wild-type control (**a**) and
890 *orion*¹ (**b**) in 6 h APF brains and the corresponding quantitation in arbitrary units (A.U.) in
891 astrocytes (**c**). Green corresponds to the expression of *201Y-GAL4* driven *UAS-mCD8-GFP* in
892 γ axons. The astrocyte cytoplasm, in which quantitation are performed, is circled by a white
893 dotted line in **a** and **b**. **c**, Quantitation of Drpr expression in arbitrary units (A.U.) reveals no
894 significant differences between control and *orion*¹. Results are means \pm S.E.M. n = 5 MBs for
895 control and 7 MBs for *orion*¹; p = 1 (Mann-Whitney *U* test). In addition, since *drpr* expression
896 is regulated by the transcription factor STAT92E⁴⁶, we analyzed the expression of an *STAT92E-*
897 *GFP* reporter in wild-type and *orion*¹. **d-f**, Expression of 10X-STAT92E-GFP (green) in wild-
898 type control (**d**) and *orion*¹ (**e**) larval brains and the corresponding quantitation in arbitrary units
899 (A.U.) (**f**). Red is both, Fas2 labelling γ axon bundles and Repo antibody labelling the glial cell
900 nuclei. Pictures are confocal Z-projections. The astrocyte cytoplasm, in which quantitation are
901 performed, is circled by a white dotted line in **d** and **e**. **f**, Quantitation of STAT-GFP expression
902 in arbitrary units (A.U.) reveals no significant differences between control and *orion*¹. Results
903 are means \pm S.E.M. n = 12 MBs for control and 10 MBs for *orion*¹; p = 0.09 (Mann-Whitney
904 *U* test). Scale bars are 30 μ m in **a**, **b** and 20 μ m in **d**, **e**. Genotypes are listed in Supplementary
905 list of fly strains.
906

907 **Supplementary list of fly strains:**

908

909 **Fig. 1: a, c-e,** $y w^{67c23} / Y$ or $y w^{67c23} / y w^{67c23}$; $UAS-mCD8GFP 201Y-GAL4/+$. **b, f-i,** $y w^{67c23}$
910 $sn^3 orion^1 FRT19A / Y$ or $y w^{67c23} sn^3 orion^1 FRT19A / y w^{67c23} sn^3 orion^1 FRT19A$; $UAS-$
911 $mCD8GFP 201Y-GAL4 / +$. **j,** $y w^{67c23} sn^3 orion^1 FRT19A / Y$; $UAS-mCD8GFP 201Y-GAL4/+$;
912 $UAS-orion-A-myc / +$. **k,** $y w^{67c23} sn^3 orion^1 FRT19A / Y$; $UAS-mCD8GFP 201Y-GAL4 / +$;
913 $UAS-orion-B-myc / +$. **l,** $y w^{67c23} / Y$ or $y w^{67c23} / w^{1118}$; $UAS-mCD8GFP 201Y-GAL4 / UAS-$
914 $orion-RNAi$.

915

916 **Fig. 3: a, b, d, e, g, h, j, k,** $y w^{67c23} / Y$ or $y w^{67c23} / y w^*$; $UAS-mCD8GFP 201Y-GAL4 / +$;
917 $UAS-orion-B-myc / +$. **c, f, i,** $y w^{67c23} / Y$ or $y w^{67c23} / y w^*$; $UAS-mCD8GFP 201Y-GAL4 / +$;
918 $UAS-orion-B-\Delta SP-myc / +$.

919

920 **Fig. 4: a, b,** $y w^{67c23} sn^3 FRT19A / Y$; $repo-GAL4 UAS-mCD8GFP / +$. **c,** $y w^{67c23} sn^3 orion^1$
921 $FRT19A / Y$; $repo-GAL4 UAS-mCD8GFP / +$. **d-g,** $y w^{67c23} / Y$ or $y w^{67c23} / y w^*$; $UAS-$
922 $mCD8GFP 201Y-GAL4 / +$; $UAS-orion-B-myc / +$. **h,** $y w^{67c23} / Y$ or $y w^{67c23} / y w^*$; $UAS-$
923 $mCD8GFP 201Y-GAL4 / +$; $UAS-orion-B-\Delta SP-myc / +$.

924

925 **Supplementary Fig. 1: a, e, h-k,** $y w^{67c23} / Y$ or $y w^{67c23} / y w^{67c23}$; $UAS-mCD8GFP 201Y-GAL4$
926 $/ +$. **b, l-o,** $y w^{67c23} sn^3 orion^1 FRT19A / Y$ or $y w^{67c23} sn^3 orion^1 FRT19A / y w^{67c23} sn^3 orion^1$;
927 $UAS-mCD8GFP 201Y-GAL4 / +$. **c,** $y w^{67c23} / Y$ or $y w^{67c23} / y w^{67c23}$; $UAS-mCD8GFP 201Y-$
928 $GAL4 / +$; $drpr^{\Delta 5} / drpr^{\Delta 5}$. **d, g,** $y w^{67c23} / Y$ or $y w^{67c23} / y w^{67c23}$; $Hr39^{C13}$, $UAS-mCD8GFP$
929 $201Y-GAL4 / +$. **f,** $y w^* orion^{\Delta C} / Y$; $UAS-mCD8GFP 201Y-GAL4 / +$. **p,** $y w^{67c23} sn^3 orion^1$
930 $FRT19A / Y$; $UAS-mCD8GFP 201Y-GAL4 / +$; $UAS-orion-B-myc / +$.

931

932 **Supplementary Fig. 2: a, e and j. WT:** $y w^{67c23} / Y$; $UAS-mCD8GFP 201Y-GAL4 / +$. **Hr39:**
933 $y w^{67c23} / Y$; $Hr39^{C13}$, $UAS-mCD8GFP 201Y-GAL4 / +$. **orion Δ C:** $y w^* orion^{\Delta C} / Y$; $UAS-$
934 $mCD8GFP 201Y-GAL4 / +$. **orion1:** $y w^{67c23} sn^3 orion^1 FRT19A / Y$; $UAS-mCD8GFP 201Y-$
935 $GAL4 / +$. **orionRNAi:** $y w^{67c23} / Y$; $UAS-mCD8GFP 201Y-GAL4 / UAS-orion-RNAi$. **drpr Δ 5:**
936 $y w^{67c23} / Y$; $UAS-mCD8GFP 201Y-GAL4 / +$; $drpr^{\Delta 5} / drpr^{\Delta 5}$. **b, f,** $y w^{67c23} / Y$; $UAS-$
937 $mCD8GFP 201Y-GAL4 / +$. **c,** $y w^{67c23} sn^3 orion^1 FRT19A / Y$; $UAS-mCD8GFP 201Y-GAL4$
938 $/ +$. **d:** $y w^{67c23} / Y$; $Hr39^{C13}$, $UAS-mCD8GFP 201Y-GAL4 / +$. **g-i, k-m,** $UAS-mCD8GFP 201Y-$
939 $GAL4 / +$; $drpr^{\Delta 5} / drpr^{\Delta 5}$. **n,** $y w^* orion^{\Delta C} / Y$; $UAS-mCD8GFP 201Y-GAL4 / +$.

940

941 **Supplementary Fig. 3: a**, $y w^{67c23} sn^3 orion^1 FRT19A / Y$; $UAS-mCD8GFP 201Y-GAL4 / +$;
942 $UAS-orion-B-myc / +$. **b**, $y w^{67c23} sn^3 orion^1 FRT19A / Y$; $UAS-mCD8GFP 201Y-GAL4 / +$;
943 $UAS-orion-B- Mut AX3C-myc / +$. **c**, $y w^{67c23} sn^3 orion^1 FRT19A / Y$; $UAS-mCD8GFP 201Y-$
944 $GAL4 / +$; $UAS-orion-B-Mut CX4C-myc- / +$. **d**, $y w^{67c23} sn^3 orion^1 FRT19A / Y$; $UAS-$
945 $mCD8GFP 201Y-GAL4 / +$; $UAS-orion-B-\Delta SP-myc / +$. **e**, $y w^{67c23} sn^3 orion^1 FRT19A / Y$;
946 $UAS-mCD8GFP 201Y-GAL4 / +$; $UAS-orion-B-Mut GAG1-myc / +$. **f**, $y w^{67c23} sn^3 orion^1$
947 $FRT19A / Y$; $UAS-mCD8GFP 201Y-GAL4 / +$; $UAS-orion-B-Mut GAG2-myc / +$. **g**, $y w^{67c23}$
948 $sn^3 orion^1 FRT19A / Y$; $UAS-mCD8GFP 201Y-GAL4 / +$; $UAS-orion-B-Mut GAG3-myc / +$. **h**,
949 **control**: $y w^{67c23} / Y$; $UAS-mCD8GFP 201Y-GAL4 / +$. **orion1**: $y w^{67c23} sn^3 orion^1 FRT19A /$
950 Y ; $UAS-mCD8GFP 201Y-GAL4 / +$. **orion1 + orion-B WT**: see above **(a)**. **orion1 + ΔSP** : see
951 above **(d)**. **orion1 + AX3C**: see above **(b)**. **orion1 + CX4C**: see above **(c)**. **orion1 + GAG1**:
952 see above **(e)**. **orion1 + GAG2**: see above **(f)**. **orion1 + GAG3**: see above **(g)**. **orion-RNAi**: y
953 w^{67c23} / Y ; $UAS-mCD8GFP 201Y-GAL4 / UAS-orion-RNAi$. **orion-RNAi + EcR-B1**: $y w^{67c23} /$
954 Y ; $UAS-mCD8GFP 201Y-GAL4 / UAS-orion-RNAi$; $UAS-EcR-B1 / +$. **orion-RNAi + control** :
955 $y w^{67c23} / Y$; $UAS-mCD8GFP 201Y-GAL4 / UAS-orion-RNAi$; $UAS-FRT-y^+-FRT / +$. **i**, 1 : y
956 $w^{67c23} sn^3 orion^1 FRT19A / Y$; $UAS-mCD8GFP 201Y-GAL4 / +$; $UAS-orion-A-myc / +$. 2 : y
957 $w^{67c23} sn^3 orion^1 FRT19A / Y$; $UAS-mCD8GFP 201Y-GAL4 / +$; $UAS-orion-B-myc / +$. 3 : y
958 $w^{67c23} sn^3 orion^1 FRT19A / Y$; $UAS-mCD8GFP 201Y-GAL4 / +$; $UAS-orion-B -\Delta SP-myc / +$.
959 4 : $y w^{67c23} sn^3 orion^1 FRT19A / Y$; $UAS-mCD8GFP 201Y-GAL4 / +$; $UAS-orion-B-Mut AX3C-$
960 $myc / +$. 5 : $y w^{67c23} sn^3 orion^1 FRT19A / Y$; $UAS-mCD8GFP 201Y-GAL4 / +$; $UAS-orion-B-$
961 $Mut CX4C-myc / +$. 6 : $y w^{67c23} sn^3 orion^1 FRT19A / Y$; $UAS-mCD8GFP 201Y-GAL4 / +$; $UAS-$
962 $orion-B-Mut GAG1-myc / +$. 7 : $y w^{67c23} sn^3 orion^1 FRT19A / Y$; $UAS-mCD8GFP 201Y-GAL4$
963 $/ +$; $UAS-orion-B -Mut GAG2-myc / +$. 8 : $y w^{67c23} sn^3 orion^1 FRT19A / Y$; $UAS-mCD8GFP$
964 $201Y-GAL4 / +$; $UAS-orion-B -Mut GAG3-myc / +$.

965
966 **Supplementary Fig. 4: b**, $y w^* orion^{\Delta A} / Y$; $UAS-mCD8GFP 201Y-GAL4 / +$. **c**, $y w^* orion^{\Delta B} /$
967 Y ; $UAS-mCD8GFP 201Y-GAL4 / +$. **d**, $y w^* orion^{\Delta C} / Y$; $UAS-mCD8GFP 201Y-GAL4 / +$.

968
969 **Supplementary Fig. 5: a**, $y w^{67c23} sn^3 orion^1 FRT19A / Y$; $CyO, P(Dfd-GMR-nvYFP)2 / +$ or
970 $Sp / +$; $alm-GAL4 UAS-mCD8GFP / +$. **b**, $y w^{67c23} sn^3 orion^1 FRT19A / Y$; $CyO, P(Dfd-$
971 $GMR-nvYFP)2 / +$ or $Sp / +$; $alm-GAL4 UAS-mCD8GFP / UAS-orion-A-myc$. **c**, $y w^{67c23} sn^3$
972 $orion^1 FRT19A / Y$; $CyO, P(Dfd-GMR-nvYFP)2 / +$ or $Sp / +$; $alm-GAL4 UAS-mCD8GFP$
973 $/ UAS-orion-B-myc$. **d**, $y w^{67c23} / Y$ or $y w^{67c23} / w^*$; $UAS-mCD8GFP 201Y-GAL4 / UAS-orion-$
974 $RNAi$. **e**, w^* / Y or w^* / w^* ; $UAS-orion-RNAi / +$; $repo-GAL4 UAS-mCD8GFP / +$.

975

976 **Supplementary Fig. 6: a**, $w^* tub-P-GAL80 hs-FLP122 FRT19A / y w^{67c23} sn^3 FRT19A ; UAS-$
977 $mCD8GFP 201Y-GAL4 / +$. **b**, $w^* tub-P-GAL80 hs-FLP122 FRT19A / y w^{67c23} sn^3 orion^1$
978 $FRT19A ; UAS-mCD8GFP 201Y-GAL4 / +$. **c**, $y w^{67c23} sn^3 orion^1 FRT19A / Y ; UAS-mCD8GFP$
979 $201Y-GAL4 / + ; UAS-EcR-B1 / +$. **d**, $y w^{67c23} sn^3 FRT19A / Y ; UAS-mCD8GFP 201Y-GAL4 /$
980 $+$. **e**, $y w^{67c23} sn^3 orion^1 FRT19A / Y ; UAS-mCD8GFP 201Y-GAL4 / +$. **g-i**, $y w^{67c23} / Y$ or y
981 $w^{67c23} / y w^{67c23} ; UAS-mCD8GFP 201Y-GAL4 / + ; 2x UAS-drl-myc / +$. **j-l**, $y w^{67c23} / Y$; or y
982 $w^{67c23} / y w^* UAS-mCD8GFP 201Y-GAL4 / + ; UAS-orion-B-myc / +$.

983

984 **Supplementary Fig. 8: a, b, e, f**, $y w^{67c23} sn^3 FRT19A / Y ; repo-GAL4 UAS-mCD8GFP / +$.
985 **c, d, g, h** $y w^{67c23} sn^3 orion^1 FRT19A / Y ; repo-GAL4 UAS-mCD8GFP / +$. **i**, w^* / Y or $w^* /$
986 w^* ; $CyO, P(Dfd-GMR-nvYFP)2 / Sp ; alrm-GAL4 UAS-mCD8GFP / alrm-GAL4 UAS-$
987 $mCD8GFP$. **j**, WT : $y w^{67c23} / Y ; CyO, P(Dfd-GMR-nvYFP)2 / +$ or $Sp / + ; alrm-GAL4 UAS-$
988 $mCD8GFP / +$. $orion^1$: $y w^{67c23} sn^3 orion^1 FRT19A / Y ; CyO, P(Dfd-GMR-nvYFP)2 / +$ or
989 $Sp / + ; alrm-GAL4 UAS-mCD8GFP / +$.

990

991 **Supplementary Fig. 9: a-f**, $y w^{67c23} / Y$ or $y w^{67c23} / y w^*$; $UAS-mCD8GFP 201Y-GAL4 / + ;$
992 $UAS-orion-B-myc / +$.

993

994 **Supplementary Fig. 10: a**, $y w^{67c23} / Y$ or $y w^{67c23} / y w^{67c23} ; UAS-mCD8GFP 201Y-GAL4 /$
995 CyO . **b**, $y w^{67c23} sn^3 orion^1 FRT19A / Y$ or $y w^{67c23} sn^3 orion^1 FRT19A / y w^{67c23} sn^3 orion^1$
996 $FRT19A ; UAS-mCD8GFP 201Y-GAL4 / CyO$. **d**, $y w^{67c23} sn^3 FRT19A / Y ; 10X-STAT92E-$
997 $GFP / +$. **e**, $y w^{67c23} sn^3 orion^1 FRT19A / Y ; 10X-STAT92E-GFP / +$.

998

999

1000

1001

1002

1003